Case Studies in Thermal Engineering 68 (2025) 105853

Contents lists available at ScienceDirect

Case Studies in Thermal Engineering

journal homepage: www.elsevier.com/locate/csite

Investigating the interactive effects of different functional parameters of a heating, cooling and power cycle based on DOE method

Reza Hajipour [a], Elaheh Neshat [a,*], Ali Shokri Kalan [b]

[a] Faculty of Mechanical Engineering, Sahand University of Technology, Sahand New Town, Tabriz, Iran
[b] Renewable Energy and Built Environment, University of Vaasa, P.O. Box 700, FIN-65101, Vaasa, Finland

HIGHLIGHTS

- A novel cogeneration system integrating the Brayton, Kalina, and lithium-bromide cycles is developed.
- Multi-objective optimization improves system efficiency and reduces total cost by 8.16 %.
- Parametric studies and DOE analysis reveal key interactions in system performance.
- The system achieves 0.8 MW power, 0.4 MW cooling, and 1.2 MW heating with competitive costs.
- Upper-limit optimization of equivalence ratio and isentropic efficiency maximizes first and second-law efficiencies.

ARTICLE INFO

Keywords:
Cogeneration systems
Design of experiment method
Interaction effects
Exergy
Exergoeconomic

ABSTRACT

Cogeneration systems reduce fuel consumption and environmental pollutants. Optimizing these systems and operating existing equipment under optimal conditions further enhances fuel savings and pollution reduction. This study aims to investigate the interaction effects of functional parameters to identify the optimal operating conditions for all components. A new cogeneration system based on the methane-burning Brayton cycle, Kalina cycle, lithium-bromide cooling cycle, and a heating unit is designed. System performance is evaluated in terms of energy, exergy, and exergoeconomics. A parametric study identifies the optimal range of functional conditions with linear output changes, and the DOE method with fractional factorial design examines component interactions and their effects on system outputs. The most significant factors are the equivalence ratio and isentropic efficiency of compressors and the gas turbine, with their upper limits maximizing first and second-law efficiencies and the utilization factor. Analyzed using FORTRAN and Minitab, the system delivers 0.8 MW power, 0.4 MW cooling, and 1.2 MW heating, with energy and power costs of $16.53 and $51.19 per MWh. Multi-objective optimization improves exergy efficiency, reduces the total cost rate by 8.16 % to $110.76/hr, and lowers LCOP and cooling costs by 11.73 % and 4.15 %, respectively.

Abbreviations

ABS	Absorber	PEC	Purchased equipment costs ($)
		$\dot{H}$	Heat rate (kW)

(*continued on next page*)

* Corresponding author.
E-mail address: e_neshat@sut.ac.ir (E. Neshat).

https://doi.org/10.1016/j.csite.2025.105853
Received 28 September 2024; Received in revised form 23 December 2024; Accepted 6 February 2025
Available online 10 February 2025

(*continued*)

CC	Combustion Chamber	$\overline{R}$	Universal gas constant (kJ/kmol.K)
COM	Compressor	s	Specific entropy (kJ/kg.K)
CON	Condenser	U	Total heat transfer coefficient (kW/ m^2 K)
ECO	Economizer	w	Lithium Bromide concentration (%)
EVA	Evaporator	$\dot{W}$	Power (kW)
GT	Gas Turbine	x	Ammonia concentration (%)
HP	High Pressure	x^0	Standard molar percentage (%)
LP	Low Pressure	Y	Exergy destruction ratio
HT	High Temperature	Y^*	Exergy destruction ratio
SHX	Solution Heat Exchanger	$\dot{Z}$	Equipment cost rate ($/h)
MIX	Mixer		
P	Pump	**Greek symbols**	
SEP	Separator	Δ	Difference
V	Valve	ε	Exergy efficiency
Latin		η	Energy efficiency
A	Heat transfer area (m^2)	ξ	Chemical exergy coefficient of fuel
BL	System life time (year)	φ	Fuel equivalence ratio
C	Unit cost ($/GJ)	ϕ	Maintenance factor
$\dot{C}$	Cost rate ($/h)	ε_{II}	Outlet
CRF	Capital Recovery Factor	**Subscripts and superscripts**	
CR	Compression Ratio	CV	Control volume
COP	Coefficient of performance	ch	chemical
$\dot{E}$	Exergy rate (kW)	D	Destruction
e^0	Standard chemical exergy (kJ/kmol)	F	Fuel
$\overline{e}$	Chemical exergy (kJ/kmol)	in	Input
f	Exergo-economic factor (%)	k	Component number
h	Specific enthalpy (kJ/kg)	L	Loss
i	Annual interest rate (%)	m	Mean
$\dot{I}$	Irreversibility	out	
LHV	Lower heating value (kJ/kg)	pp	Pinch point
LMTD	Logarithmic mean temperature difference (K)	ph	Physical
LCOE	Unit cost rate of produced energy ($/MWh)	p	Product
LCOP	Unit cost rate of production power ($/MWh)	r	refrigerant
$\dot{m}$	Mass flow rate (kg/s)	th	Thermal
M	Molecular Weight (kg)	tot	Total
N	Number of working hours (h)	v	vapor

1. Introduction

Today, as the population grows and the demand for energy continues to rise, energy production has become a vital aspect of society [1]. Consequently, numerous power generation facilities have been established and put into operation in the recent years [2]. Releasing exhaust gases into the environment is a significant contributor to global warming and an even greater cause of energy waste [3]. Implementing waste heat recovery technology is highly beneficial in preventing energy loss. The waste heat from thermal power units, often referred to as low-temperature energy, can be effectively utilized to drive multi-generation energy systems, such as Combined Heat and Power (CHP) and Combined Cooling, Heating, and Power (CCHP) units, thereby enhancing overall energy efficiency [4]. These highly efficient CHP units are widely promoted worldwide. They can be powered by various sources including fuel cells [5], gas turbines [6], micro-turbines [7], and steam turbines [8], utilizing both fossil fuels [9] and renewable energy [10]. As a subsystem in CCHP systems, various configurations use different subsystems such as the Organic Rankine Cycle [11,12], Refrigeration Cycle [13,14], Kalina Cycle [15], desalination cycle [16], Brayton [17] or a combination of them. Given the numerous studies on CCHP systems, it is beneficial to explore and further develop these systems.

Enhancing combined generation cycles and establishing optimal operational parameters constitutes the approach employed to enhance the efficiency of such systems. Various optimization methods have been explored for enhancing CCHP systems [18]. Genetic Algorithm stands out as the most widely utilized approach for optimizing energy systems [19]. In this algorithm, objective functions are categorized into single-objective and multi-objective functions [20]. In several studies, this algorithm has been used to optimize cogeneration cycles with two prime movers [21], offshore platforms [22], PEMFC systems [23], and systems driven by exhaust gases from internal combustion engines [24]. When this algorithm is used, an optimal operational mode is estimated for each component. If all components operate in their optimal mode, objective functions such as thermal efficiency and cost rate [25], exergy efficiency [26], and fresh water production and electricity rate [27] will be optimized. In addition to the genetic algorithm, other optimization algorithms have been used to optimize cogeneration cycles, including Response Surface Methodology (RSM) for optimizing hydrogen production rate [28] and electricity rate [29], Multi-Objective Particle Swarm Optimization (MOPSO) for single renewable-based energy systems [30] and hybrid systems [31], Multi-Objective Multi-Verse Optimizer (IMOMVO) [32], Grey Wolf Algorithm [33], and Artificial Bee Colony (ABC) Algorithm [34].The most important problem of all the mentioned methods is that all these methods produce optimal point responses, which means that all components must operate at their optimal point to achieve the optimal objective. In addition, the interaction between the operational modes of different components cannot be investigated in these methods,

and therefore an optimal operational range cannot be defined for the system. Therefore, it is necessary to analyze the interaction between different components in order to provide an optimal performance range for the system based on the performance of each component [35]. In several engineering problems, the interactive effects of different parameters have been studied [35,36].

One approach that investigates the correlation between multiple input variables and output responses is the design of experiments (DOE) method. Employing this method offers the benefit of minimizing tests while enabling the measurement of interaction effects among various variables on the system response. Unlike the mentioned optimization algorithms, the DOE method does not yield specific numerical values for each parameter; instead, it evaluates their relative importance, interference, and qualitative effects in comparison to one another. This method finds application in numerous engineering scenarios where optimizing output responses based on input parameters is essential [15,37]. From the literature review, significant research has focused on designing and analysing combined cooling, heating, and power (CCHP) systems. Most studies propose CCHP configurations that fall short of maximum efficiency. This work introduces an efficient CCHP system emphasizing waste heat recovery, incorporating LiBr-Water absorption refrigeration, and Brayton and Kalina subsystems. While many systems undergo various optimization methods, the primary goal of this research is to develop an effective cogeneration system that generates electricity, cooling, and heating while reducing costs, minimizing irreversibility, and enhancing efficiency. Key contributions include determining the sequence of bottoming cycle connections, optimizing cooling, heating, and power outputs, adjusting component operating conditions, applying the DOE method for system optimization, and analysing parameter interactions. These findings help define the optimal performance range for the proposed system, leading to reduced energy consumption.

2. Methodology

2.1. System configuration and description

The proposed system consists of three sections: Brayton, absorption refrigeration, and Kalina cycles, as shown in Fig. 1. In the Brayton cycle, ambient air enters COM1 (state 1), is compressed to 3 bar (state 2), and its thermal energy is harnessed via HX1. HX1 acts as a cooler for the Brayton cycle and a generator for the absorption refrigeration cycle, which uses water as the refrigerant and lithium bromide as the absorbent. Heating the Lithium-Bromide/Water solution in HX1 separates water vapor (state 38), which is condensed (state 39), expanded through V.3, and enters the evaporator (state 40), absorbing heat and producing cooling (states 46–47). The water (state 41) is absorbed by the lithium bromide solution (state 34), which is cooled (states 44–45), pressurized by pump 3 (state 35), and returned to HX1 via SHX.

Air exiting HX1 (state 3) is compressed in COM2 (state 4), and after combustion, high-temperature exhaust gases (state 5) drive the gas turbine, generating power. The exhaust gases (state 6) contain useable thermal energy, which is harnessed in the HP EVA of the

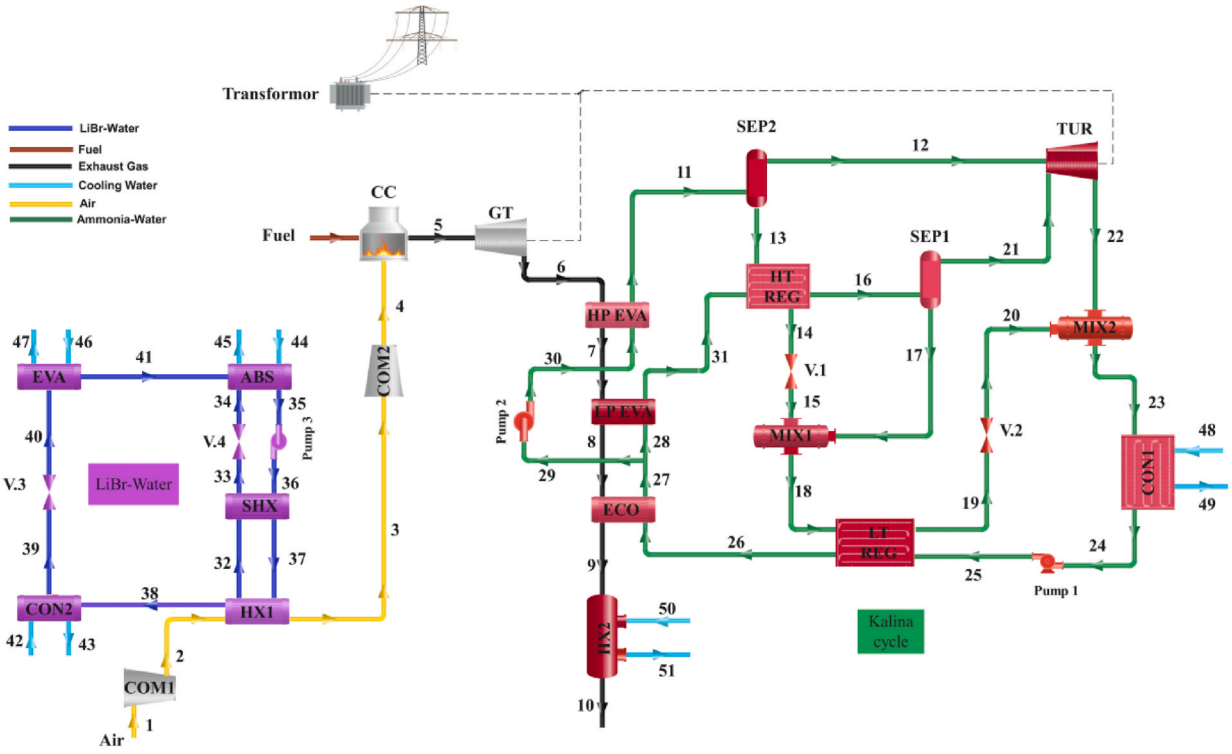

Fig. 1. The schematic diagram of the proposed system.

Kalina cycle. The vapor from SEP 1 (state 12) and state 21 expands in the turbine to generate power. The solution from MIX 1 (state 18) exchanges heat in LT REG, is expanded through V.2, mixes with the turbine output (state 22) in MIX 2, and enters CON1. The condenser output (state 24) is pressurized by pump P1 and heated in ECO (state 26). The heated solution (state 27) splits into two streams: one is pressurized by pump 2 (state 29) and sent to HP EVA (state 11), while the other is sent to LP EVA (state 28). Residual exhaust heat from ECO (state 9) is used for heating purposes via a heat exchanger.

2.2. Inputs, assumptions and mathematical model of the proposed system

- The Energy, Exergy, and Thermo-economic modeling of the proposed cogeneration system are performed using Fortran software, and for optimization, Minitab is utilized. In this section, thermodynamic models for each component of the proposed system are discussed, and the following assumptions are outlined below:
- Methane (CH_4) is used as the fuel, and it has a Lower Heating Value of 50 MJ/kg.
- All studied processes are assumed to be steady-state flows.
- Heat losses are neglected in all heat exchangers.
- The potential pressure drops in the streams and pipes are disregarded.
- Compressors, pumps, and turbines operate under adiabatic conditions.
- The reference temperature and pressure are considered to be 298.15 K and 1 bar, respectively.
- The kinetic and potential energies are negligible.
- The thermodynamic properties of the lithium bromide-water solution have been calculated using the equations provided by Patek et al. [38].
- The thermodynamic properties of ammonia-water solution have been obtained using the equations provided by Wang [39].
- The air composition has been considered with a suitable approximation consisting of 79 % nitrogen and 21 % oxygen.
- Air and combustion products are assumed to be an ideal gas.
- The thermodynamic properties of air and combustion products have been calculated using the relations provided by McBride and others [40].

There are some performance and design parameters which are taken as inputs and presented in Table 1.

2.3. Energy analysis

The equations of the mass and energy conservation laws are expressed as follows [41]:

$$\sum \dot{m}_{in} = \sum \dot{m}_{out} \tag{1}$$

$$\dot{Q}_{CV} + \sum \dot{m}_{in} h_{in} = \dot{W}_{CV} + \sum \dot{m}_{out} h_{out} \tag{2}$$

Table 2 illustrates the energy and mass balance for all components.

2.3.1. Brayton cycle

It is assumed that complete combustion has occurred between fuel and air in the combustion chamber of the Brayton cycle. The stoichiometric combustion equation of methane is presented as below:

Table 1
The input data.

Input data	Unit	Value
Brayton		
Mass flow rate of air	kg/s	3
Isentropic efficiency of COM 1, 2	%	80
Isentropic efficiency of Gas Turbine	%	90
Air-Fuel equivalence ratio	–	0.34
Compression ratio	–	3
Li-Br/Water absorption refrigeration cycle		
Temperature of ABS	K	310.95
Temperature of CON 2	K	310.95
Temperature of EVA	K	283.15
Isentropic efficiency of pump3	%	90
Kalina cycle		
Ammonia concentration of basic solution		0.6
Mid-cycle pressure of the Kalina cycle	bar	15
Maximum pressure of the Kalina cycle	bar	25
Temperature of CON 1	K	308.15
Isentropic efficiencies of pump 1, 2	%	0.7

Table 2
Mass, concentration and energy balances equations.

Components	Equations
Brayton	
COM 1	$\eta_{COM1} = \frac{T_{2s} - T_1}{T_2 - T_1}, \dot{W}_{COM1} = \dot{m}_{air}(h_2 - h_1), \dot{m}_{air} = \dot{m}_1 = \dot{m}_2$
HX1	$\dot{Q}_{HX1} = \dot{m}_{air}(h_2 - h_3)\ \dot{m}_{air}(h_2 - h_3) = \dot{m}_{38}h_{38} + \dot{m}_{32}h_{32} - \dot{m}_{37}h_{37}$ $\dot{m}_{38} = \dot{m}_r, \dot{m}_{32} = \dot{m}_{34}, \dot{m}_{37} = \dot{m}_{35}, \dot{m}_3 = \dot{m}_2$
COM 2	$\eta_{COM2} = \frac{T_{4s} - T_3}{T_4 - T_3}, \dot{W}_{COM2} = \dot{m}_{air}(h_4 - h_3), \dot{m}_4 = \dot{m}_3$
CC	$\dot{m}_5 h_5 = \dot{m}_4 h_4 + \dot{m}_{fuel} LHV_{fuel}, \dot{m}_5 = \dot{m}_{air} + \dot{m}_{fuel}$
GT	$\eta_{GT} = \frac{T_5 - T_6}{T_5 - T_{6s}}, \dot{W}_{GT} = \dot{m}_6(h_5 - h_6), \dot{m}_6 = \dot{m}_5$
Absorption refrigeration cycle	
CON2	$\dot{Q}_{CON2} = \dot{m}_{38}(h_{38} - h_{39}),\ \dot{m}_{38}(h_{38} - h_{39}) = \dot{m}_{42}(h_{43} - h_{42})\ \dot{m}_{39} = \dot{m}_{38}, \dot{m}_{43} = \dot{m}_{42}$
Valve 3	$\dot{m}_{39} = \dot{m}_{38}, \dot{m}_{43} = \dot{m}_{42}\ , \dot{m}_{40} = \dot{m}_{39}$
EVA	$\dot{Q}_{EVA} = \dot{m}_{40}(h_{41} - h_{40})\ \dot{m}_{40}(h_{41} - h_{40}) = \dot{m}_{46}(h_{46} - h_{47})$ $\dot{m}_{41} = \dot{m}_{40}, \dot{m}_{46} = \dot{m}_{47}$
ABS	$\dot{Q}_{abs} = \dot{m}_{44}(h_{45} - h_{44})\ \dot{m}_{44}(h_{45} - h_{44}) = \dot{m}_{41}h_{41} + \dot{m}_{34}h_{34} - \dot{m}_{35}h_{35}$ $\dot{m}_{34}w_{34} = \dot{m}_{35}w_{35},\ \dot{m}_{35} = \dot{m}_{34} + \dot{m}_{41}, \dot{m}_{45} = \dot{m}_{44}$
Valve 4	$h_{34} = h_{33}\ , w_{34} = w_{33}, \dot{m}_{34} = \dot{m}_{33}$
Pump3	$\eta_{Pump3} = \frac{h_{36} - h_{35}}{h_{36s} - h_{35}}$ $\dot{W}_{Pump3} = \dot{m}_{35}(h_{36} - h_{35})\ , w_{35} = w_{36}, \dot{m}_{35} = \dot{m}_{36}$
SHX	$\epsilon_{SHX} = \frac{h_{33} - h_{32}}{\acute{h}_{33} - h_{32}}\ , \acute{h}_{33} = h(x_{33}, T_{36})$ $\dot{Q}_{SHX} = \dot{m}_{36}(h_{37} - h_{36})\ w_{37} = w_{36}, w_{32} = w_{33}, \dot{m}_{37} = \dot{m}_{36}, \dot{m}_{32} = \dot{m}_{33}$
Kalina	
HP EVA	$\dot{Q}_{HP\ EVA} = \dot{m}_6(h_6 - h_7)\ \dot{m}_6(h_6 - h_7) = \dot{m}_{11}(h_{11} - h_{30})$ $x_{30} = x_{11} = x_{bs}\ , \dot{m}_{30} = \dot{m}_{11} = \frac{\dot{m}_{bs}}{2}$
Pump 2	$\eta_{Pump2} = \frac{h_{30} - h_{29}}{h_{30s} - h_{29}}$ $\dot{W}_{Pump2} = \dot{m}_{29}(h_{30} - h_{29})\ x_{29} = x_{30}\ , \dot{m}_{29} = \dot{m}_{30}$
LP EVA	$\dot{Q}_{LP\ EVA} = \dot{m}_7(h_7 - h_8), \dot{m}_7(h_7 - h_8) = \dot{m}_{28}(h_{31} - h_{28})\ x_{31} = x_{28} = x_{bs}, \dot{m}_8 = \dot{m}_7, \dot{m}_{31} = \dot{m}_{28} = \frac{\dot{m}_{bs}}{2}$
ECO	$\dot{Q}_{ECO} = \dot{m}_8(h_8 - h_9)\ \dot{m}_8(h_8 - h_9) = \dot{m}_{27}(h_{27} - h_{26})$ $x_{27} = x_{26}, \dot{m}_9 = \dot{m}_8, \dot{m}_{27} = \dot{m}_{26}$
SEP 2	$\dot{m}_{11}h_{11} = \dot{m}_{12}h_{12} + \dot{m}_{13}h_{13}$ $\dot{m}_{11}x_{11} = \dot{m}_{12}x_{12} + \dot{m}_{13}x_{13}$ $\dot{m}_{11} = \dot{m}_{12} + \dot{m}_{13}$
Valve 1	$h_{15} = h_{14}\ , x_{15} = x_{14}\ , \dot{m}_{15} = \dot{m}_{14}$
HT REG	$\dot{Q}_{HT\ REG} = \dot{m}_{31}(h_{16} - h_{31})\ \dot{m}_{31}(h_{16} - h_{31}) = \dot{m}_{13}(h_{13} - h_{14})$ $x_{16} = x_{31}, x_{13} = x_{14}$ $\dot{m}_{14} = \dot{m}_{13}, \dot{m}_{16} = \dot{m}_{31}$
SEP 1	$\dot{m}_{16}h_{16} = \dot{m}_{21}h_{21} + \dot{m}_{17}h_{17}$ $\dot{m}_{16}x_{16} = \dot{m}_{21}x_{21} + \dot{m}_{17}x_{17}$ $\dot{m}_{16} = \dot{m}_{21} + \dot{m}_{17}$
MIX 1	$\dot{m}_{15}h_{15} = \dot{m}_{17}h_{17} + \dot{m}_{18}h_{18}$ $\dot{m}_{15}x_{15} = \dot{m}_{17}x_{17} + \dot{m}_{18}x_{18}$ $\dot{m}_{15} = \dot{m}_{17} + \dot{m}_{18}$
MIX 2	$\dot{m}_{22}h_{22} = \dot{m}_{20}h_{20} + \dot{m}_{23}h_{23}$ $\dot{m}_{22}x_{22} = \dot{m}_{20}x_{20} + \dot{m}_{23}x_{23}$ $\dot{m}_{22} = \dot{m}_{20} + \dot{m}_{23}$
CON 1	$\dot{Q}_{CON1} = \dot{m}_{23}(h_{23} - h_{24})\ \dot{m}_{23}(h_{23} - h_{24}) = \dot{m}_{48}(h_{49} - h_{48})$ $\dot{m}_{24} = \dot{m}_{23} = \dot{m}_{bs}, \dot{m}_{48} = \dot{m}_{49}$ $x_{23} = x_{24} = x_{bs}$
Pump1	$\eta_{Pump1} = \frac{h_{25} - h_{24}}{h_{25s} - h_{24}}$ $\dot{W}_{Pump1} = \dot{m}_{24}(h_{25} - h_{24})\ x_{25} = x_{24}$ $\dot{m}_{25} = \dot{m}_{24}$
Valve 2	$h_{20} = h_{19}, x_{20} = x_{19}, \dot{m}_{20} = \dot{m}_{19}$
LT REG	$\dot{Q}_{LT\ REG} = \dot{m}_{25}(h_{26} - h_{25})\ \dot{m}_{25}(h_{26} - h_{25}) = \dot{m}_{19}(h_{18} - h_{19})$ $x_{25} = x_{26}, x_{19} = x_{18}$ $\dot{m}_{26} = \dot{m}_{25}, \dot{m}_{19} = \dot{m}_{18}$
HX 2	$\dot{Q}_{HX2} = \dot{m}_9(h_9 - h_{10})\ \dot{m}_9(h_9 - h_{10}) = \dot{m}_{50}(h_{51} - h_{50})$ $\dot{m}_{10} = \dot{m}_9, \dot{m}_{51} = \dot{m}_{50}$
TUR	$\dot{W}_{TUR} = \dot{m}_{21}h_{21} + \dot{m}_{12}h_{12} - \dot{m}_{22}h_{22}$ $\eta_{TUR} = \frac{-\dot{m}_{22}h_{22} + \dot{m}_{12}h_{12} + \dot{m}_{21}h_{21}}{-\dot{m}_{22}h_{22s} + \dot{m}_{12}h_{12} + \dot{m}_{21}h_{21}}\ \dot{m}_{22} = \dot{m}_{21} + \dot{m}_{12}$

$$CH_4 + 2(O_2 + 3.76N_2) \rightarrow CO_2 + 2H_2O + 7.52N_2 \quad (3)$$

Assuming a lean mixture, the combustion equation of methane is shown as follow:

$$CH_4 + 2 \Big/ \phi(O_2 + 3.76N_2) \rightarrow CO_2 + 2H_2O + 2\left({}^{1}/_{\phi} - 1\right)O_2 + {}^{7.52}/_{\phi}N_2 \quad (4)$$

By applying proportionality relations between fuel, air, and other gases, the following relations are obtained:

$$\dot{m}_{fuel} = 0.0584 \times \phi \times \dot{m}_{air} \quad (5)$$

$$\dot{m}_{CO_2} = 0.1606 \times \phi \times \dot{m}_{air} \quad (6)$$

$$\dot{m}_{H_2O} = 0.1314 \times \phi \times \dot{m}_{air} \quad (7)$$

$$\dot{m}_{O_2} = 0.9344 \times \phi \times \dot{m}_{air} \quad (8)$$

$$\dot{m}_{N_2} = 0.7669 \times \phi \times \dot{m}_{air} \quad (9)$$

Where, ϕ is an indicator of the air-fuel equivalence ratio and, $\dot{m}_{fuel}$ and $\dot{m}_{air}$ are expressed as mass flow rate of fuel and air, respectively.

2.3.2. Absorption refrigeration cycle

For the thermodynamic analysis of the single-effect lithium bromide-Water absorption refrigeration cycle used in the system, in addition to the mass and energy conservation equations, the conservation of mass concentration of lithium bromide in the HX1 or the ABS is also applied.

$$\sum (\dot{m}w)_{in} = \sum (\dot{m}w)_{out} \quad (10)$$

where, **w** illustrates the lithium bromide concentration of the solution and is defined as below:

$$w = \frac{\dot{m}_{LiBr}}{\dot{m}_{(LiBr+Water)}} \quad (11)$$

2.3.3. Kalina cycle

For the Kalina cycle applied in the proposed system, in addition to the energy and mass conservation equations, the balance of ammonia concentration should also be applied as follows:

$$\sum (\dot{m}x)_{in} = \sum (\dot{m}x)_{out} \quad (12)$$

where x represents the ammonia concentration of the solution and is defined as follows:

$$\boldsymbol{x} = \frac{\dot{\boldsymbol{m}}_{\boldsymbol{NH_3}}}{\dot{\boldsymbol{m}}_{(\boldsymbol{NH_3}+\boldsymbol{Water})}} \quad (13)$$

2.3.4. Heating unit

The heating unit of the proposed system is HX2, a shell-and-tube heat exchanger specifically designed to generate the required hot water. Heat from the exhaust gas is transferred to the intermediate fluid, which is water entering and exiting at temperatures of 25 °C and 65 °C, respectively.

By considering all the definitions, the equations concerning mass, concentration, and energy balances for each component in the proposed system are included in Table 2.

2.3.5. Coefficient of performance of an absorption refrigeration cycle

The Coefficient of Performance (COP) of the absorption refrigeration system represents the efficiency of the desired absorption chiller, which is equal to the ratio of the heat extracted from the intended space to the input power.

$$COP_{Absorption} = \frac{\dot{Q}_{cooling}}{\dot{Q}_{in} + \dot{W}_{pump3}} \quad (14)$$

$$\dot{Q}_{cooling} = \dot{Q}_{EVA} \quad (15)$$

$$\dot{Q}_{in} = \dot{Q}_{HX1} \quad (16)$$

2.3.6. The efficiency of the first law of thermodynamics

The efficiency of the first law or the thermal efficiency of the overall system is defined as follows:

$$\eta_{th} = \frac{\dot{W}_{net} + \dot{Q}_{cooling} + \dot{Q}_{heating}}{\dot{m}_{fuel} \times LHV_{fuel}} \tag{17}$$

$$\dot{W}_{net} = \dot{W}_{GT} + \dot{W}_{TUR} - \dot{W}_{COM1} - \dot{W}_{COM2} - \dot{W}_{pump1} - \dot{W}_{pump2} - \dot{W}_{pump3} \tag{18}$$

$$\dot{Q}_{heating} = \dot{Q}_{HX2} \tag{19}$$

2.4. Exergy analysis

In exergy analysis, an attempt is made to simultaneously apply the first and second laws of thermodynamics and, by considering the surroundings as a reference state, obtain the maximum work produced in the system [15].

In the absence of nuclear, magnetic, electrical, and surface tension effects, the total exergy of a system can be divided into four components: physical exergy, kinetic exergy, potential exergy, and chemical exergy. As mentioned, in the present study, the effects of kinetic and potential exergy are neglected, and only chemical and physical exergy are considered.

$$\dot{E} = \dot{E}_{ph} + \dot{E}_{ch} \tag{20}$$

Physical exergy refers to the maximum useful work that can be produced by a system as it comes into equilibrium with the environment.

$$\dot{E}_{ph} = \dot{m}(h - h_0) - T_0(s - s_0) \tag{21}$$

Where, h_0 and s_0 represent enthalpy and entropy at reference conditions, respectively.

And chemical exergy is the amount of work achievable from a substance under ambient conditions, wherein the substance undergoes a chemical reaction with the components of the environment, and the reaction products ultimately reach a dead state [24].

The chemical exergy of fuel used in proposed system can be approximately calculated as follows:

$$\xi = \frac{Ex_f}{LHV_f} \tag{22}$$

Which, for hydrocarbons with the general formula C_xH_y, the value of ξ is calculated as bellows [42]:

$$\xi = 1.033 + 0.0169\frac{y}{x} - \frac{0.0698}{x} \tag{23}$$

The ratio of chemical exergy to the lower heating value is typically close to 1 for gaseous fuels, commonly around one. For methane fuel, this ratio is approximately 1.06 [43].

To determine the chemical exergy of the ammonia/water solution employed in the Kalina cycle, the equation provided below is utilized [42]:

$$\dot{E}_{ch,NH_3/H_2O} = \dot{m}\left\{\left(\frac{x}{M_{NH3}}\right)e^0_{ch,NH_3} + \left(\frac{1-x}{M_{H2o}}\right)e^0_{ch,H_2O}\right\} \tag{24}$$

Where, M_{NH3} and M_{H2O} are molar mass of ammonia and water, and also e^0_{ch,NH_3} and e^0_{ch,H_2O} indicate the standard chemical exergies of ammonia and water. The chemical exergy of the water and lithium bromide solution is also obtained using the following equation [44]:

$$\dot{E}_{ch,LiBr/Water} = \dot{m}\{49.4342 + 4.2369 \times 100w + 0.0705 \times (100w)^2\} \tag{25}$$

where w represents the mass concentration of lithium bromide in the solution. The chemical exergy of water is also obtained in kJ/kmol according to the following equation [45]:

$$\bar{e}_{ch} = \bar{R}T_0 \ln\left(\frac{P_g(T_0)}{x_v^0 \times P_0}\right) \tag{26}$$

In the provided equation, x_v^0 denotes the standard molar percentage of water vapor in the air, and $P_g(T_0)$ is the saturation pressure of water at the reference temperature [44]. In addition, for calculating the chemical exergy of an ideal gas mixture, the following equation is employed [44]:

$$\bar{e}_{ch} = \sum x_i \bar{e}_{ch,i} + \bar{R}T_0 \sum x_i \ln(x_i) \tag{27}$$

In the mentioned equation, x_i represents the molar percentage of components, and $\bar{e}_{ch,i}$ denotes the standard chemical exergy of the mixture components.

2.4.1. Exergy destruction

The destruction of exergy, or the irreversibility of each component, is defined based on the following relationship [10.1016/j.enconman.2023.116669]:

$$\dot{E}_F = \dot{E}_p + \dot{E}_D + \dot{E}_L \tag{28}$$

In order, $\dot{E}_L$, $\dot{E}_D$, $\dot{E}_P$ and $\dot{E}_F$ are related to exergy losses, exergy destruction, product exergy, and fuel exergy. Given the exclusion of heat losses, the value of exergy destruction in the current work is zero. The expressions for the ratios of exergy destruction of each component to the input exergy of the fuel to the system Y_D and the ratio of exergy destruction of each component to the total exergy destruction of the system Y_D^* are provided as follows:

$$Y_D = \frac{\dot{E}_{D,i}}{\dot{E}_{fuel}} \tag{29}$$

$$Y_D^* = \frac{\dot{E}_{D,i}}{\dot{E}_{D,tot}} \tag{30}$$

And exergy efficiency for each component is defined as follows:

$$\eta_{ex,i} = \frac{\dot{E}_{p,i}}{\dot{E}_{F,i}} \tag{31}$$

Also the exergy efficiency of the proposed system is calculated as follows:

$$\eta_{II} = \frac{\dot{W}_{net}}{\dot{E}_{fuel}} \tag{32}$$

$$\dot{W}_{net} = \dot{W}_{GT} + \dot{W}_{TUR} - \dot{W}_{COM1} - \dot{W}_{COM2} - \dot{W}_{pump1} - \dot{W}_{pump2} - \dot{W}_{pump3} \tag{33}$$

And the Utilization Factor is defined as the sum of exergies achievable from the chemical exergy of the fuel which is shown as follows:

Table 3
The equations concerning the exergy balance of each component.

Components	Exergy Balance
Brayton	
COM 1	$\dot{E}_{D,COM1} = \dot{E}_1 - \dot{E}_2 + \dot{W}_{COM1}$
HX1	$\dot{E}_{D,HX1} = \dot{E}_2 + \dot{E}_{37} - \dot{E}_3 - \dot{E}_{32} - \dot{E}_{38}$
COM 2	$\dot{E}_{D,COM2} = \dot{E}_3 - \dot{E}_4 + \dot{W}_{COM2}$
CC	$\dot{E}_{D,CC} = \dot{E}_{Fuel} + \dot{E}_4 - \dot{E}_5$
GT	$\dot{E}_{D,GT} = \dot{E}_5 - \dot{E}_6 - \dot{W}_{GT}$
Absorption refrigeration cycle	
CON2	$\dot{E}_{D,CON2} = \dot{E}_{38} + \dot{E}_{42} - \dot{E}_{39} - \dot{E}_{43}$
Valve 3	$\dot{E}_{D,exp.v3} = \dot{E}_{39} - \dot{E}_{40}$
EVA	$\dot{E}_{D,EVA} = \dot{E}_{40} + \dot{E}_{46} - \dot{E}_{41} - \dot{E}_{47}$
ABS	$\dot{E}_{D,ABS} = \dot{E}_{41} + \dot{E}_{44} + \dot{E}_{34} - \dot{E}_{45} - \dot{E}_{35}$
Valve 4	$\dot{E}_{D,V.4} = \dot{E}_{33} - \dot{E}_{34}$
Pump3	$\dot{E}_{D,pump3} = \dot{E}_{35} - \dot{E}_{36} + \dot{W}_{pump3}$
SHX	$\dot{E}_{D,SHX} = \dot{E}_{32} + \dot{E}_{36} - \dot{E}_{33} - \dot{E}_{37}$
Kalina	
HP EVA	$\dot{E}_{D,HP\ EVA} = \dot{E}_{30} + \dot{E}_6 - \dot{E}_{11} - \dot{E}_7$
Pump 2	$\dot{E}_{D,pump2} = \dot{E}_{29} - \dot{E}_{30} + \dot{W}_{pump2}$
LP EVA	$\dot{E}_{D,LP\ EVA} = \dot{E}_7 + \dot{E}_{28} - \dot{E}_{31} - \dot{E}_8$
ECO	$\dot{E}_{D,ECO} = \dot{E}_8 + \dot{E}_{26} - \dot{E}_9 - \dot{E}_{27}$
SEP 2	$\dot{E}_{D,SEP2} = \dot{E}_{11} - \dot{E}_{12} - \dot{E}_{13}$
Valve 1	$\dot{E}_{D,V.1} = \dot{E}_{14} - \dot{E}_{15}$
HT REG	$\dot{E}_{D,HT\ REG} = \dot{E}_{13} + \dot{E}_{31} - \dot{E}_{14} - \dot{E}_{16}$
SEP 1	$\dot{E}_{D,SEP\ 1} = \dot{E}_{16} - \dot{E}_{17} - \dot{E}_{21}$
MIX 1	$\dot{E}_{D,MIX\ 1} = \dot{E}_{15} + \dot{E}_{17} - \dot{E}_{18}$
MIX 2	$\dot{E}_{D,mix2} = \dot{E}_{20} + \dot{E}_{22} - \dot{E}_{23}$
CON 1	$\dot{E}_{D,CON1} = \dot{E}_{23} + \dot{E}_{48} - \dot{E}_{24} - \dot{E}_{49}$
Pump1	$\dot{E}_{D,pump1} = \dot{E}_{24} - \dot{E}_{25} + \dot{W}_{pump1}$
Valve 2	$\dot{E}_{D,V.2} = \dot{E}_{19} - \dot{E}_{20}$
LT REG	$\dot{E}_{D,LT\ REG} = \dot{E}_{18} + \dot{E}_{25} - \dot{E}_{19} - \dot{E}_{26}$
HX 2	$\dot{E}_{D,HX2} = \dot{E}_9 + \dot{E}_{50} - \dot{E}_{10} - \dot{E}_{51}$
TUR	$\dot{E}_{D,TUR} = \dot{E}_{12} + \dot{E}_{21} - \dot{E}_{22} - \dot{W}_{TUR}$

$$\varepsilon_{II}(UF) = \frac{\dot{W}_{net} + \dot{E}_{P,EVA} + \dot{E}_{P,HX2}}{\dot{E}_{fuel}} \tag{34}$$

The equations concerning the exergy balance of each component are outlined in Table 3.

2.5. Exergo-economic analysis

For the exergoeconomic analysis of the proposed system in this study, the Specific Exergy Cost method, proposed by Lazzaretto et al. [46], has been employed. According to this approach, a cost balance equation is formulated for each component, where the costs of the output streams of a component are equal to the sum of the input costs plus the capital investment and maintenance costs for that component.

In general, the cost balance equation for each component of the system under consideration is as follows [47]:

$$\sum (\dot{C}_i)_{in} + \sum (\dot{C}_i)_Q + \dot{Z} = \sum (\dot{C}_i)_{out} + \sum (\dot{C}_i)_W \tag{35}$$

Where $\dot{C}_i$ is the cost rate of each stream. In the SPECO approach, every stream is assigned a distinct cost determined directly by its exergy value. Consequently, the exergy cost is computed as follows for both the inlet and outlet streams:

$$\dot{C}_i = c_i \dot{E}_i \tag{36}$$

Where, c_i is the average cost per unit of exergy. Moreover, $\dot{Z}$ represents the total expenses encompassing the investment allocation x, along with the operating and maintenance costs y, outlined as follows:

$$\dot{Z}_k = \dot{Z}_k^{CI} + \dot{Z}_k^{OM} = PEC_K.CRF.\frac{\varphi}{N} \tag{37}$$

$$CRF = \frac{i(1+i)^{BL}}{(1+i)^{BL} - 1} \tag{38}$$

In which, PEC represents the purchase cost of the specific component in US dollars. The capital recovery factor, CRF, is responsible for accounting for capital recovery, while φ (with a value of 1.06) is used to denote the maintenance factor. N is assigned to represent the annual working hours for the component, assumed to be 8000 h. The annual interest rate, denoted by i, is specified, and BL represents the useful life of the power plant in years. These values are set at 12 % and 20 years, respectively [48].

For converting the equipment purchase cost from the base year to the current year, the CEPCI index is utilized, as described by the following equation [48]:

Table 4
The correlations applied for the purchased equipment cost of the components.

Component	PEC ($)	Ref
COM 1,2	$\frac{71.1 \times \dot{m}_{air}}{0.9 - \eta_{COM}} \times CR \times \ln CR$	[44]
CC	$\frac{46.08 \times \dot{m}_{air}}{0.995 - \frac{P_5}{P_4}} \times \left(1 + e^{(0.018 \times T_5 - 36.4)}\right)$	[44]
GT	$\frac{479.34 \times \dot{m}_{gas}}{0.92 - \eta_{GT}} \times \ln\left(\frac{P_5}{P_6}\right) \times \left(1 + e^{(0.036 \times T_5 - 54.4)}\right)$	[44]
HX 1	$12000 \times \left(\frac{A_{HX1}}{100}\right)^{0.6}$	[51]
CON 1	$8000 \times \left(\frac{A_{CON1}}{100}\right)^{0.6}$	[52]
EVA	$16000 \times \left(\frac{A_{EVA}}{100}\right)^{0.6}$	[52]
ABS	$16500 \times \left(\frac{A_{ABS}}{100}\right)^{0.6}$	[52]
Pump3	$2100 \times \left(\frac{\dot{W}_{pump3}}{10}\right)^{0.26} \times \left(\frac{1 - \eta_{pump3}}{\eta_{pump3}}\right)^{0.5}$	[51]
SHX	$12500 \times \left(\frac{A_{SHX}}{100}\right)^{0.6}$	[52]
Pump 1,2	$1120 \times \dot{W}_{pump}^{0.8}$	[53]
TUR	$4405 \times \dot{W}_{TUR}^{0.7}$	[53]
Kalina heat exchangers	$2143 \times A^{0.514}$	[50]
All expansion valves	300	[51]

$$PEC_k = PEC_{ref} \times \left(\frac{CI_{new}}{CI_{ref}}\right) \tag{39}$$

The indices *new* and *ref* are associated with the cost index of the reference year and the current year, respectively [49]. The relationships used to estimate the purchase cost of various equipment in the studied system are presented in Table 4. The purchase cost of separators and mixers is marginal compared to other components; therefore, their purchase cost is disregarded [50].

The heat transfer surface area (A) is a crucial parameter in the assessment of the Purchase Equipment Cost (PEC) for most heat exchangers. This is elaborated as follows:

$$A = \frac{\dot{Q}}{U \times LMTD} \tag{40}$$

In which, U and LMTD denote the overall heat transfer coefficient of the heat exchangers and the logarithmic mean temperature difference, respectively. To calculate the overall heat transfer coefficients for heat exchangers, values provided in various references are applied, as outlined in Table 5:

To calculate the logarithmic mean temperature difference for not countercurrent flows, the following equation has been used for all the heat exchangers:

$$LMTD = \frac{\left(T_{hot,in} - T_{cold,out}\right) - \left(T_{hot,out} - T_{cold,in}\right)}{\ln \frac{T_{hot,in} - T_{cold,out}}{T_{hot,out} - T_{cold,in}}} \tag{41}$$

The equations related to the cost balance for all components of the system, along with the auxiliary equations, are presented in Table 6.

In the present study, the average cost per unit of exergy for methane fuel is considered to be 3.284 $/GJ, as indicated in Ref. [55]. Therefore, the cost of methane fuel is determined as follows:

$$\dot{C}_{fuel} = \dot{m}_{fuel} \times c_{fuel} \times LHV_{fuel} \tag{42}$$

With the given cost rates and exergy rates for fuel and product in each system component, the unit cost of exergy for fuel $\left(c_{F,k}\right)$ and the unit cost of exergy for the product $\left(c_{P,k}\right)$ associated with that specific component are determined based on the following relationships:

$$c_{F,k} = \frac{\dot{C}_{F,k}}{\dot{E}_{F,k}} \tag{43}$$

$$c_{P,k} = \frac{\dot{C}_{P,k}}{\dot{E}_{P,k}} \tag{44}$$

Given that the overall cost of a system component is equivalent to the sum of investment, maintenance, and exergy destruction costs, the Exergy-Economic Factor (f) is utilized to ascertain the proportion of each of these costs in the system components.

$$f_k = \frac{\dot{Z}_k}{\dot{Z}_k + \dot{C}_{D,k} + \dot{C}_{L,k}} \tag{45}$$

The total cost rate of the proposed system, along with the economic evaluation of the proposed system, involves the calculation of the levelized cost of energy and power (LCOE-LCOP) are described as follows:

$$\dot{C}_{sys} = \sum \dot{Z}_k + \dot{C}_{fuel} \tag{46}$$

Table 5
Overall heat transfer coefficients.

Equipment	$U\left(\frac{kw}{m^2k}\right)$	Ref
SHX	0.13	[51]
EVA	0.2	[51]
CON2	3.2	[51]
ABS	0.4	[51]
HX1	2.3	[51]
ECO	0.13	[54]
LT-HT REG	1	[54]
LP-HP EVA	0.9	[54]
HX2	1.1	[54]
CON1	1.1	[54]

Table 6
The cost rate balance and the auxiliary equations of the components.

Component	Cost Balance equation	Auxiliary relation
COM 1	$c_1\dot{E}_1 + c_{w,COM1}\dot{W}_{COM1} + \dot{Z}_{COM1} = c_2\dot{E}_2$	$c_1 = 0$
HX1	$c_{37}\dot{E}_{37} + c_2\dot{E}_2 + \dot{Z}_{HX1} = c_{32}\dot{E}_{32} + c_{38}\dot{E}_{38} + c_3\dot{E}_3$	$\frac{c_{32}\dot{E}_{32} - \left(\frac{\dot{m}_{32}}{\dot{m}_{37}}\right)c_{37}\dot{E}_{37}}{\dot{E}_{32} - \left(\frac{\dot{m}_{32}}{\dot{m}_{37}}\right)\dot{E}_{37}} = \frac{c_{38}\dot{E}_{38} - \left(\frac{\dot{m}_{38}}{\dot{m}_{37}}\right)c_{37}\dot{E}_{37}}{\dot{E}_{38} - \left(\frac{\dot{m}_{38}}{\dot{m}_{37}}\right)\dot{E}_{37}}$
		$c_2 = c_3$
COM 2	$c_3\dot{E}_3 + c_{w,COM2}\dot{W}_{COM2} + \dot{Z}_{COM2} = c_4\dot{E}_4$	–
CC	$c_4\dot{E}_4 + \dot{Z}_{CC} + \dot{C}_{fuel} = c_5\dot{E}_5$	–
GT	$c_5\dot{E}_5 + \dot{Z}_{GT} = c_6\dot{E}_6 + c_{w,GT}\dot{W}_{GT}$	$c_5 = c_6$
		$c_{w,comp1} = c_{w,comp2} = c_{w,pump3} = c_{w,GT}$
CON 2	$c_{38}\dot{E}_{38} + c_{42}\dot{E}_{42} + \dot{Z}_{CON2} = c_{39}\dot{E}_{39} + c_{43}\dot{E}_{43}$	$c_{42} = 0$
		$c_{38} = c_{39}$
Exp. Valve3	$c_{39}\dot{E}_{39} + \dot{Z}_{exp.v3} = c_{40}\dot{E}_{40}$	–
EVA	$c_{40}\dot{E}_{40} + c_{46}\dot{E}_{46} + \dot{Z}_{EVA} = c_{41}\dot{E}_{41} + c_{47}\dot{E}_{47}$	$c_{46} = 0$
		$c_{40} = c_{41}$
ABS	$c_{41}\dot{E}_{41} + c_{34}\dot{E}_{34} + c_{44}\dot{E}_{44} + \dot{Z}_{ABS} = c_{35}\dot{E}_{35} + c_{45}\dot{E}_{45}$	$c_{44} = 0$
		$c_{35} = \frac{c_{34}\dot{E}_{34} + c_{41}\dot{E}_{41}}{\dot{E}_{34} + \dot{E}_{41}}$
Exp. Valve 4	$c_{33}\dot{E}_{33} + \dot{Z}_{exp.v4} = c_{34}\dot{E}_{34}$	–
Pump3	$c_{35}\dot{E}_{35} + c_{w,pump3}\dot{W}_{pump3} + \dot{Z}_{pump3} = c_{36}\dot{E}_{36}$	–
SHX	$c_{32}\dot{E}_{32} + c_{36}\dot{E}_{36} + \dot{Z}_{SHX} = c_{33}\dot{E}_{33} + c_{37}\dot{E}_{37}$	$c_{32} = c_{33}$
Pump 2	$c_{29}\dot{E}_{29} + c_{w,pump2}\dot{W}_{pump2} + \dot{Z}_{pump2} = c_{30}\dot{E}_{30}$	
HP EVA	$c_6\dot{E}_6 + c_{30}\dot{E}_{30} + \dot{Z}_{HP\ EVA} = c_7\dot{E}_7 + c_{11}\dot{E}_{11}$	$c_6 = c_7$
LP EVA	$c_7\dot{E}_7 + c_{28}\dot{E}_{28} + \dot{Z}_{LP\ EVA} = c_8\dot{E}_8 + c_{31}\dot{E}_{31}$	$c_7 = c_8$
ECO	$c_8\dot{E}_8 + c_{26}\dot{E}_{26} + \dot{Z}_{ECO} = c_9\dot{E}_9 + c_{27}\dot{E}_{27}$	$c_9 = c_8$,
		$c_{28} = 0.5c_{27}$, $c_{29} = 0.5c_{27}$
SEP 2	$c_{11}\dot{E}_{11} = c_{12}\dot{E}_{12} + c_{13}\dot{E}_{13}$	$c_{12} = c_{13}$
Exp. Valve 1	$c_{14}\dot{E}_{14} + \dot{Z}_{exp.v1} = c_{15}\dot{E}_{15}$	–
HT REG	$c_{13}\dot{E}_{13} + c_{31}\dot{E}_{31} + \dot{Z}_{HT\ REG} = c_{16}\dot{E}_{16} + c_{14}\dot{E}_{14}$	$c_{13} = c_{14}$
SEP 1	$c_{16}\dot{E}_{16} = c_{17}\dot{E}_{17} + c_{21}\dot{E}_{21}$	$c_{21} = c_{17}$
MIX 1	$c_{15}\dot{E}_{15} + c_{17}\dot{E}_{17} = c_{18}\dot{E}_{18}$	–
MIX 2	$c_{20}\dot{E}_{20} + c_{22}\dot{E}_{22} = c_{23}\dot{E}_{23}$	–
CON 1	$c_{23}\dot{E}_{23} + c_{48}\dot{E}_{48} + \dot{Z}_{CON1} = c_{24}\dot{E}_{24} + c_{49}\dot{E}_{49}$	$c_{48} = 0$
		$c_{23} = c_{24}$
Pump 1	$c_{24}\dot{E}_{24} + c_{w,pump1}\dot{W}_{pump1} + \dot{Z}_{pump1} = c_{25}\dot{E}_{25}$	–
Exp. Valve 1	$c_{19}\dot{E}_{19} + \dot{Z}_{exp.v2} = c_{20}\dot{E}_{20}$	
LT REG	$c_{18}\dot{E}_{18} + c_{25}\dot{E}_{25} + \dot{Z}_{LT\ REG} = c_{19}\dot{E}_{19} + c_{26}\dot{E}_{26}$	$c_{18} = c_{19}$
HX2	$c_9\dot{E}_9 + c_{50}\dot{E}_{50} + \dot{Z}_{HX2} = c_{10}\dot{E}_{10} + c_{51}\dot{E}_{51}$	$c_{50} = 0$
		$c_9 = c_{10}$
TUR	$c_{12}\dot{E}_{12} + c_{21}\dot{E}_{21} + \dot{Z}_{TUR} = c_{22}\dot{E}_{22} + c_{w,Tur}\dot{W}_{TUR}$	$c_{12} + c_{21} = c_{22}$
		$c_{w,pump1} = c_{w,pump2} = c_{w,Tur}$

$$LCOE\left(\$/MWh\right) = \left(\frac{\dot{C}_{sys}}{\dot{W}_{net} + \dot{Q}_{heating} + \dot{Q}_{cooling}}\right) \times 1000 \tag{47}$$

$$LCOP\left(\$/MWh\right) = \left(\frac{\dot{C}_{sys}}{\dot{W}_{net}}\right) \times 1000 \tag{48}$$

2.6. Evaluation of the interaction of components using the DOE method

The design of experiments (DOE) is a critical tool in industries and laboratories, enabling reliable results, time savings, fewer experiments, and process optimization. Unlike the classical method, which changes one parameter at a time while keeping others constant, DOE examines the effects of multiple variables simultaneously, including their interactions. This approach highlights the importance and interplay of parameters without directly providing optimized values, offering a more comprehensive understanding of system behavior.

The DOE method selects the smallest possible number of trials leading to accurate results. Selection of factors, determination of factor levels and ranges, and selection of response variables are the most important variables to determine before using the DOE method. Equivalence ratio, gas turbine isentropic efficiency, isentropic efficiency of compressors, isentropic efficiency of the turbine, and evaporator temperature are factors in this study. First and second law efficiency and levelized cost of energy are considered as the main outputs. After selecting factors and response variables, screening is done. The purpose of screening is to find out which factors are more efficient in the processor, which allows to optimize these factors [56]. Screening can be done using two methods, full factorial

design (FD) and fractional factorial design (FFD) [57]. One of the most important factor modeling methods is the two-level K-factor. These factors can be quantitative or qualitative. In factorization, the first step is to indicate the higher and lower levels and the number of moves obtained based on the following equation [56–58]:

$$\text{Number of RUN} = L^{f} \tag{49}$$

where f is number of factors and L is level. When dealing with many factors, the fractional factorial method is preferred over the full factorial method to reduce the number of runs and associated costs. Fractional factorial designs require significantly fewer experiments compared to full factorial designs. In this study, the number of experiments for the fractional factorial design is calculated using the following equation [58].:

$$\text{Number of RUN} = L^{f-1} \tag{50}$$

Then at first values of high and low levels of parameters should be selected. The range of parameters changes are selected based on the parametric study results. Then the selected ranges are used for evaluating the interaction between parameters.

3. Result and discussion

In this section, the discussion proceeds after validating all three components of the system: Brayton, refrigeration absorption, and Kalina cycle. The outcomes of the energy, exergy, and exergo-economic analyses are then presented. Subsequently, the results obtained from the optimization using the Design of Experiments (DOE) method are also provided.

3.1. Verification

To validate the modeling conducted for the Brayton, refrigeration absorption, and Kalina cycles, the thermodynamic characteristics of these cycles were compared with those of similar cycles found in the referenced works [59–61]. The results are presented in Tables 7–9.

3.2. Energy and exergy analysis

In this section, the results of the thermodynamic analysis of the studied system in the base case are provided in detail. The power production of the system in this state is 0.8 MW, and the cooling and heating capacities are 0.4 and 1.2 MW, respectively. The overall energy and exergy results of the system are presented in Table 10.

The results related to the exergy analysis of the system components in the baseline condition, including the values related to exergy destruction, the contribution of exergy destruction for each component relative to the total exergy destruction, and the exergy efficiency of the components, are presented in Table 11. As observed in the table, the highest level of exergy destruction is associated with the combustion chamber, accounting for approximately 55 % of the total exergy destruction in the system. This is due to the occurrence of chemical reactions in the CC and the creation of a significant temperature difference. Following the combustion chamber, HX2, compressors, and other heat exchangers contribute the most to exergy destruction. This is attributed to factors such as the low efficiency of compressors and the temperature difference between the input and output of heat exchangers. The ABS demonstrates the lowest exergy efficiency, and HX 2, along with the HP and LP EVAs, also exhibits low efficiencies.

Fig. 2 illustrates the distribution of exergy destruction among the three cycles constituting the overall system. As depicted in the figure, the gas turbine cycle shows the highest share of exergy destruction. Following the gas turbine cycle, the Kalina cycle ranks second, contributing to the highest exergy destruction with a 24 % share. The absorption refrigeration cycle exhibits the lowest exergy destruction, accounting for 5 %.

3.3. Exergo-economic analysis

The results of exergoeconomic analysis in the baseline condition for all points of the cycle are presented in Table 12.

As indicated in Table 13, the highest investment and maintenance costs are associated with the gas turbine and the absorber of the absorption refrigeration system, respectively.

Table 7
Comparing the Brayton results with those of Mohammadi et al. [61].

State	T(K)			P(bar)			$\dot{m}$ (kg/s)		
	Present work	[61]	(%)	Present work	[61]	(%)	Present work	[61]	(%)
1	298.15	298.15	0	1.01	1.01	0	0.1	0.1	0
2	435.38	434.88	0.1	3.193	3.19	0.09	0.1	0.1	0
3	311.15	313.15	0.6	3.161	3.16	0.03	0.1	0.1	0
4	454.09	457.59	0.7	10.1	10	1	0.1	0.1	0
5	1073.15	1073.15	0	9.99	10	0.1	0.102	0.102	0
6	658	665.12	1	1.04	1.04	0	0.102	0.102	0

Table 8
Comparing the refrigeration absorption cycle with the [60].

State	T(K)			P(bar)			w(%)			$\dot{m}$ (kg/s)		
	Present work	[60]	(%)	Present work	[60]	(%)	Present work	[60]	(%)	Present work	[60]	(%)
1	310.95	310.95	0	1.0101	1.0101	0	55.37	55.42	0.09	8.99	9.035	0.5
2	310.95	310.95	0	0.068	0.0655	4.5	55.37	55.42	0.09	8.99	9.035	0.5
3	337.75	339.35	0.7	0.068	0.065	4	55.37	55.42	0.09	8.99	9.035	0.5
4	360.95	360.95	0	0.068	0.065	4	62.30	62.32	0.03	7.99	8.035	0.56
5	326.51	326.23	0.1	0.068	0.065	4	62.30	62.32	0.03	7.99	8.035	0.56
6	326.51	326.23	0.1	1.0101	1.0101	0	62.30	62.32	0.03	7.99	8.035	0.56
7	360.95	360.95	0	0.068	0.0655	3.8	–	–		1	1	0
8	310.95	310.95	0	0.0683	0.0655	4.2	–	–		1	1	0
9	280.43	280.35	0.02	0.0101	0.0101	0	–	–		1	1	0
10	280.35	280.35	0	0.0101	0.0101	0	–	–		1	1	0

Table 9
Comparison between the reference system and the Kalina cycle applied in the present study [59].

State	T(K)			x			P(bar)			$\dot{m}$ (kg/s)		
	Present work	[59]	(%)	Present work	[59]	(%)	Present work	[59]	(%)	Present work	[59]	(%)
1	370.69	371.17	0.12	0.6	0.6	0	15	15	0	0.15	0.15	0
2	370.69	371.17	0.12	0.955	0.96	0.52	15	15	0	0.054	0.055	1.81
3	370.69	371.17	0.12	0.398	0.391	1.79	15	15	0	0.095	0.095	0
4	365	364.5	0.13	0.6	0.6	0	15	15	0	0.15	0.15	0
5	373	372.5	0.13	0.347	0.351	1.13	25	25	0	0.0817	0.083	1.56
6	373.1	372.62	0.12	0.347	0.351	1.13	15	15	0	0.0817	0.083	1.56
7	371.95	371.96	0.002	0.375	0.372	0.8	15	15	0	0.177	0.178	0.56
8	323.84	321.78	0.64	0.375	0.372	0.8	15	15	0	0.177	0.178	0.56
9	323.9	321.9	0.62	0.375	0.372	0.8	6.55	6.95	5.75	0.177	0.178	0.56
10	340.73	340.88	0.04	0.6	0.6	0	6.55	6.95	5.75	0.3	0.3	0
11	405.15	405.15	0	0.6	0.6	0	25	25	0	0.15	0.15	0
12	405.15	405.15	0	0.902	0.909	0.77	25	25	0	0.068	0.067	1.49
13	405.15	405.15	0	0.347	0.351	1.13	25	25	0	0.0817	0.083	1.56
14	348.39	350.32	0.55	0.926	0.932	0.64	6.55	6.95	5.75	0.122	0.122	0
15	308.15	308.15	0	0.6	0.6	0	6.55	6.95	5.75	0.3	0.3	0
16	309.88	308.32	0.5	0.6	0.6	0	15	15	0	0.3	0.3	0
17	338.18	337.09	0.32	0.6	0.6	0	15	15	0	0.3	0.3	0
18	338.35	337.09	0.37	0.6	0.6	0	15	15	0	0.15	0.15	0
19	338.79	337.35	0.42	0.6	0.6	0	25	25	0	0.15	0.15	0
20	413.15	413.15	0	–	–	–	1	1	0	3	3	0
21	373	372.5	0.13	–	–	–	1	1	0	3	3	0
22	348.5	347.55	0.27	–	–	–	1	1	0	3	3	0
23	348.5	347.55	0.27	–	–	–	1	1	0	3	3	0

By simultaneously solving the cost balance equations and auxiliary equations, the costs of all states in the system are calculated and presented in Table 12.

As shown in Table 13, the average fuel cost per unit of exergy (c_f) for the LT REG, HT REG, and TUR is lower than that of other components, resulting in a lower exergy destruction cost rate for these components. Table 13 also presents the Exergy-Economic Factor (f), where a higher value indicates a larger share of investment cost in the total component cost, while a lower value signifies a higher cost due to exergy destruction ($\dot{C}_D$). The lowest Exergy-Economic Factor values are observed for the CC and HX1.

The total investment and exergy destruction costs are another important parameter mentioned in the specified table. According to Tables 13 and it is evident that the total costs $\dot{Z} + \dot{C}_D$ are higher for the CC, HX2, and the GT, respectively. Therefore, these components are considered the most critical components from the exergy-economic perspective. Considering the Exergy-Economic Factor for these components, it becomes clear that the high costs in the CC and HX2 are mainly due to high exergy destruction costs, while for the GT, the majority of costs are associated with investment.

Table 14 presents the overall performance results of the system. Although, with the optimization of the specified cycle, the efficiency of the Kalina cycle has increased by about 20 % compared to the reference state, the gas turbine still accounts for the majority of the total cycle power generation. Other cycle results are provided in the table below.

3.4. Evaluating upper and lower bounds of parameters

In energy generation system analyses, key objectives must be maximized or minimized. This section conducts a parametric study to determine the parameter bounds for DOE. The charts use $/h for total cost rate and $/MWh for LCOP and LCOE. Six parameters are analyzed: air-fuel equivalence ratio, isentropic efficiencies of COM 1 and 2, isentropic efficiency of the GT, isentropic efficiency of the

Table 10
Thermodynamic modeling of the proposed system.

state	Working fluid	T(K)	P(bar)	$\dot{m}$ (kg/s)	$\dot{E}_{ph}$ (kW)	$\dot{E}_{ch}$ (kW)	$\dot{E}$ (kW)
1	Air	298.15	1	3	0	0	0
2	Air	455.9	3	3	389.77	0	389.77
3	Air	285.9	3	3	283.23	0	283.23
4	Air	437.43	9	3	652.87	0	652.87
5	Exhaust gas	1026.79	8.55	3.06	2343.73	257.65	2601.39
6	Exhaust gas	640.89	1	3.06	524.59	257.65	782.24
7	Exhaust gas	600.89	1	3.06	439.29	257.65	696.95
8	Exhaust gas	580.89	1	3.06	399.14	257.65	656.79
9	Exhaust gas	560.89	1	3.06	360.72	257.65	618.37
10	Exhaust gas	306.15	1	3.06	0.93	257.65	258.59
11	Ammonia-water	367.48	25	0.58	72.56	6951.62	7024.19
12	Ammonia-water	367.48	25	0.07	31.63	1375.14	1406.77
13	Ammonia-water	367.48	25	0.51	40.92	5576.48	5617.4
14	Ammonia-water	351.54	25	0.51	34.11	5576.48	5610.59
15	Ammonia-water	346.50	15	0.51	33.36	5576.48	5609.84
16	Ammonia-water	346.61	15	0.58	60.03	6951.62	7011.65
17	Ammonia-water	346.61	15	0.5	29.34	5365.17	5394.52
18	Ammonia-water	346.58	15	1.01	62.70	10941.6	110034.36
19	Ammonia-water	333.13	15	1.01	53.21	10941.6	10994.87
20	Ammonia-water	318.39	6.55	1.01	49.97	10941.6	10991.62
21	Ammonia-water	346.61	15	0.08	30.73	1586.45	1617.18
22	Ammonia-water	303.24	6.55	0.15	39.21	2961.59	3000.8
23	Ammonia-water	317.95	6.55	1.16	89	13903.25	13992.25
24	Ammonia-water	308.15	6.55	1.16	76.78	13903.25	13980.02
25	Ammonia-water	309.88	15	1.16	78.17	13903.25	13981.42
26	Ammonia-water	324.12	15	1.16	82.7	13903.25	13985.94
27	Ammonia-water	338.36	15	1.16	90.59	13903.25	13993.84
28	Ammonia-water	338.36	15	0.58	45.29	6951.62	6996.92
29	Ammonia-water	338.36	15	0.58	45.29	6951.62	6996.92
30	Ammonia-water	338.80	25	0.58	46.09	6951.62	6997.72
31	Ammonia-water	343.54	15	0.58	54.79	6951.62	7006.41
32	Li-Br/Water	360.95	0.068	0.99	−1.87	585.23	583.36
33	Li-Br/Water	356.44	0.068	0.99	−2.68	585.23	582.55
34	Li-Br/Water	356.44	0.016	0.99	−2.68	585.23	582.55
35	Li-Br/Water	310.95	0.016	1.16	0.59	555.41	556
36	Li-Br/Water	310.98	0.068	1.16	0.59	555.41	556
37	Li-Br/Water	314.09	0.068	1.16	0.95	555.41	5556.36
38	Water	360.95	0.068	0.16	18.69	8	26.69
39	Water	310.95	0.068	0.16	0.16	8	8.16
40	Water	283.29	0.016	0.16	−0.43	8	7.57
41	Water	283.15	0.016	0.16	−14.17	8	−6.17
42	Water	298.15	1	4.77	0	238.63	238.63
43	Water	318.15	1	4.77	12.83	237.63	251.46
44	Water	298.15	1	24.06	0	1203.03	1203.03
45	Water	303.15	1	24.06	4.18	1203.03	1207.21
46	Water	298.15	1	5.99	0	299.69	299.69
47	Water	283.15	1	5.99	9.84	299.69	309.53
48	Water	298.15	1	4.51	0	225.45	225.45
49	Water	313.95	1	4.51	7.64	225.45	233.09
50	Water	298.15	1	7.72	0	385.96	395.96
51	Water	338.15	1	7.72	79.63	385.96	465.6

Kalina turbine (TUR), and evaporator temperature. The air-fuel equivalence ratio (ϕ) significantly influences system performance. As shown in Fig. 3, increasing ϕ improves first-law efficiency, second-law efficiency, and the Utilization Factor (UF) while reducing LCOP and LCOE. However, it also raises the overall cost rate of the system. It is important to note that due to temperature constraints at the GT inlet, the equivalence ratio cannot be increased arbitrarily.

The influence of the isentropic efficiency of COM1 on the system's performance conditions is illustrated in Fig. 4. As depicted, an increase in this parameter results in reduced power consumption for this component, subsequently leading to increased net power production, as well as improvements in first and second-law efficiencies and the utilization factor (UF). Moreover, the rise in the isentropic efficiency of COM1 corresponds to an increase in the total cost rate, while the increase in the levelized cost of power (LCOP) is not significant, and the levelized cost of energy (LCOE) remains approximately unchanged.

The variations in first law efficiency, second law efficiency, exergy efficiency, total cost rate, LCOP, and LCOE in relation to the isentropic efficiency of COM2 are depicted in Fig. 5. As observed in the figure, the patterns of changes in these parameters closely resemble those observed for COM1.

As shown in Fig. 6, increasing the GT's isentropic efficiency improves its performance, boosting net power generation and reducing

Table 11
Results of exergy analysis for each component.

Component	$\dot{E}$ (kW)	Y_D^* (%)	$\eta_{ex,i}$
COM1	101.7	5.8	79.41
HX1	52.84	3.03	50.4
COM2	100.63	5.77	78.6
CC	964.8	55.3	72.96
GT	80.8	4.63	95.56
CON2	5.7	0.33	69.25
Expansion valve3	0.6	0.034	92.68
EVA	3.9	0.22	71.6
ABS	16.2	0.93	20.51
SHX	0.45	0.026	44.08
HP EVA	58.82	3.37	31.03
Pump2	0.04	0.002	95.02
LP EVA	30.66	1.76	23.65
ECO	30.53	1.75	20.54
Expansion valve1	0.76	0.043	100
HT REG	1.57	0.09	76.96
CON1	4.59	0.26	62.46
Pump1	0.93	0.054	60
Expansion valve 2	3.25	0.18	100
LT REG	4.96	0.28	47.73
HX2	280.15	16	22.13
TUR	0.46	0.027	97.98

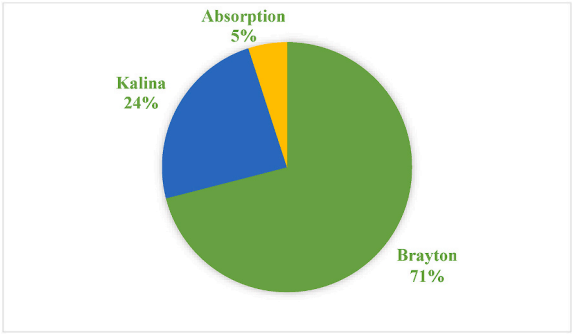

Fig. 2. Exergy destruction contribution in different part of proposed system.

exergy destruction. This also enhances both first and second law efficiencies. However, higher isentropic efficiency raises turbine investment costs, slightly increasing the system's total cost rate. Meanwhile, the Utilization Factor (UF) shows a moderate rise, and higher isentropic efficiency reduces LCOP while LCOE remains relatively constant.

Given the limited contribution of the TUR to the overall power output, enhancing its isentropic efficiency has a marginal effect on the system's performance. As illustrated in Fig. 7, the augmented power generation of the Kalina turbine (TUR) leads to a minor increase in first-law efficiency, second-law efficiency, the levelized cost of Energy (LCOE), and the utilization factor. Within the defined range of isentropic efficiency variations, the total cost rate of the system remains relatively stable, and the levelized cost of power (LCOP) undergoes a slight reduction.

Fig. 8 illustrates the impact of evaporator temperature on the selective objectives which are important. Assuming the operation of the evaporator under isobaric and isothermal conditions and considering the calculations, changes in the evaporator temperature are not anticipated to have a significant impact on the system's performance. As expected, the values of first-law efficiency, second-law efficiency, and the Utilization Factor (UF) remain relatively constant. Furthermore, a slight increase in the total cost rate leads to a marginal rise in both the Levelized Cost of Energy (LCOE) and the Levelized Cost of Power (LCOP).

3.5. System analysis using the DOE method

In this section, screening and modeling of the process will be carried out using Minitab17 software. For this purpose, three methods are available for screening: the full factorial method, the fractional factorial method, and the Plackett-Burman method. To apply the two-level full factorial screening method, the number of potential states is equal to 2^k, where k represents the number of input variables. In the present study, the number of examined parameters is 6, including the air-fuel equivalence ratio, isentropic efficiencies of COM1 and COM2, GT efficiency, Kalina turbine efficiency, and evaporator temperature. Therefore, 64 code runs are required for the two-level full factorial design method. In this study, higher-order interactions among parameters (interactions involving more than

Table 12
Exergo-economic analysis of the proposed system.

state	Working fluid	$\dot{E}$ (kW)	$\dot{C}$ ($/h)	c ($/GJ)
1	Air	0	0	0
2	Air	389.77	11.4237	8.1412
3	Air	283.23	8.3011	8.1412
4	Air	652.87	19.2502	8.1904
5	Exhaust gas	2601.39	54.4766	5.817
6	Exhaust gas	782.24	16.3811	5.817
7	Exhaust gas	696.95	14.5951	5.817
8	Exhaust gas	656.79	13.7542	5.817
9	Exhaust gas	618.37	12.9496	5.817
10	Exhaust gas	258.59	5.4152	5.817
11	Ammonia-water	7024.19	4.7067	0.1861
12	Ammonia-water	1406.77	0.9426	0.1861
13	Ammonia-water	5617.4	3.7641	0.1861
14	Ammonia-water	5610.59	3.7595	0.1861
15	Ammonia-water	5609.84	3.7673	0.1865
16	Ammonia-water	7011.65	3.7907	0.1506
17	Ammonia-water	5394.52	2.9164	0.1502
18	Ammonia-water	11004.36	6.6837	0.1687
19	Ammonia-water	10994.87	6.6779	0.1687
20	Ammonia-water	10991.62	6.6857	0.1690
21	Ammonia-water	1617.18	0.8743	0.1502
22	Ammonia-water	3000.8	3.6331	0.3363
23	Ammonia-water	13992.25	10.3187	0.2048
24	Ammonia-water	13980.02	10.3097	0.2048
25	Ammonia-water	13981.42	10.4136	0.2069
26	Ammonia-water	13985.94	10.5002	0.2085
27	Ammonia-water	13993.84	11.3748	0.2258
28	Ammonia-water	6996.92	2.8437	0.1129
29	Ammonia-water	6996.92	2.8437	0.1129
30	Ammonia-water	6997.72	2.8855	0.1145
31	Ammonia-water	7006.41	3.7101	0.1471
32	Li-Br/Water	583.36	76.6074	36.4779
33	Li-Br/Water	582.55	76.5007	36.4779
34	Li-Br/Water	582.55	76.5085	36.4815
35	Li-Br/Water	556	73.7045	36.8229
36	Li-Br/Water	556	73.7106	36.8258
37	Li-Br/Water	556.36	73.84	36.8667
38	Water	26.69	0.3851	4.0079
39	Water	8.16	0.1178	4.0079
40	Water	7.57	0.1255	4.6088
41	Water	6.17	0.1024	4.6088
42	Water	239.63	0	0
43	Water	251.46	0.3017	0.3333
44	Water	1203.03	0	0
45	Water	1207.21	2.9635	0.6819
46	Water	299.69	0	0
47	Water	309.53	1.4186	1.2731
48	Water	225.45	0	0
49	Water	233.09	0.3413	0.4067
50	Water	385.96	0	0
51	Water	465.6	7.7275	4.6103

three parameters) have been neglected, and half of the total number of runs, which is 32, has been considered. This reduced FD method is referred to as FFD (Fractional Factorial Design). In this method, the total number of runs is equal to 2^{k-r}. In the present work, due to considering runs as half, r is set to 1. Consequently, the total number of runs is reduced to 32.

In Table 15, the selected parameters, along with their upper and lower bounds, are presented. The parameter ranges have been selected based on the results of the parametric study.

By selecting the upper and lower bounds and entering them into Minitab17 software, 32 runs are generated based on the combination of various upper and lower limit values for input parameters. For evaluating the system performance, 32 simulations have been conducted, and the system outputs, including first-law efficiency, second-law efficiency, the Utilization Factor, total cost rate, the levelized cost of energy (LCOE), and the levelized cost of power, have been calculated as the system responses in Table 16. The output parameter values for each run, representing the responses, are recorded in the table. Subsequently, a statistical analysis was conducted to assess the extent of the main parameters' influence and their interaction effects on the responses.

Table 13
Exergo-economic analysis for components.

components	$\dot{Z}\left(\$/h\right)$	$\dot{C}_D\left(\$/h\right)$	$\dot{Z}+\dot{C}_D\left(\$/h\right)$	$f(\%)$	$c_f\left(\$/GJ\right)$	$c_p\left(\$/GJ\right)$
COM1	0.1028	2.3310	2.4338	4.22	6.4067	8.1412
HX1	0.03	1.5488	1.5788	1.9	8.1412	16.3081
COM2	0.1028	2.3210	2.4237	4.24	6.4067	8.2281
CC	0.0899	14.7058	14.7957	0.61	4.2372	5.8170
GT	1.9982	1.6921	3.6903	54.14	5.8170	6.4067
CON2	0.0344	0.0822	0.1166	29.49	4.0079	6.5314
V.3	0.0077	0.0086	0.0164	47.3	4.0079	4.6088
EVA	1.1907	0.06476	1.2554	94.84	4.6088	40.0641
ABS	0.2619	2.1473	2.4093	10.87	26.8229	196.9027
SHX	0.0227	0.0597	0.0824	27.53	36.4773	100.3390
HP EVA	0.03523	1.2318	1.2670	2.78	5.8170	19.1151
Pump 2	0.0223	0.0009	0.0233	95.89	6.4067	14.4649
LP EVA	0.0255	0.6420	0.6675	3.81	5.8171	25.3416
ECO	0.0700	0.6393	0.7094	9.88	5.8170	30.7870
V.1	0.0077	0.0005	0.0082	93.86	0.1861	0.1865
HT REG	0.0761	0.0010	0.0772	98.64	0.1861	4.2766
CON1	0.3323	0.0034	0.3357	98.9	0.2048	12.4128
Pump 1	0.0502	0.0216	0.0718	69.97	6.4067	20.7437
V.2	0.0077	0.0019	0.0097	79.69	0.1687	0.1690
LT REG	0.0808	0.0030	0.0838	96.40	0.1687	5.3073
HX2	0.1931	5.8667	6.060	3.18	5.8170	26.9548
TUR	0.8943	0.0004	0.8947	98.9	0.2719	21.7942

Table 14
Results in baseline condition.

Parameter	value
Produced power ($\dot{w}_{net}$)	796.7 kW
Cooling capacity ($\dot{Q}_{Cooling}$)	377.6 kW
Heating capacity ($\dot{Q}_{Heating}$)	1292 kW
COP of refrigeration absorption cycle	0.71
First law efficiency (η_I)	26.8 %
Second law efficiency (η_{II})	27.3 %
Utilization Factor (UF)	31.3 %
Total cost rate ($\dot{C}_{sys}$)	40.58 $/h
Levelized Cost Of Energy (LCOE)	16.53 $/MWh
Levelized Cost Of Power (LCOP)	51.2 $/MWh

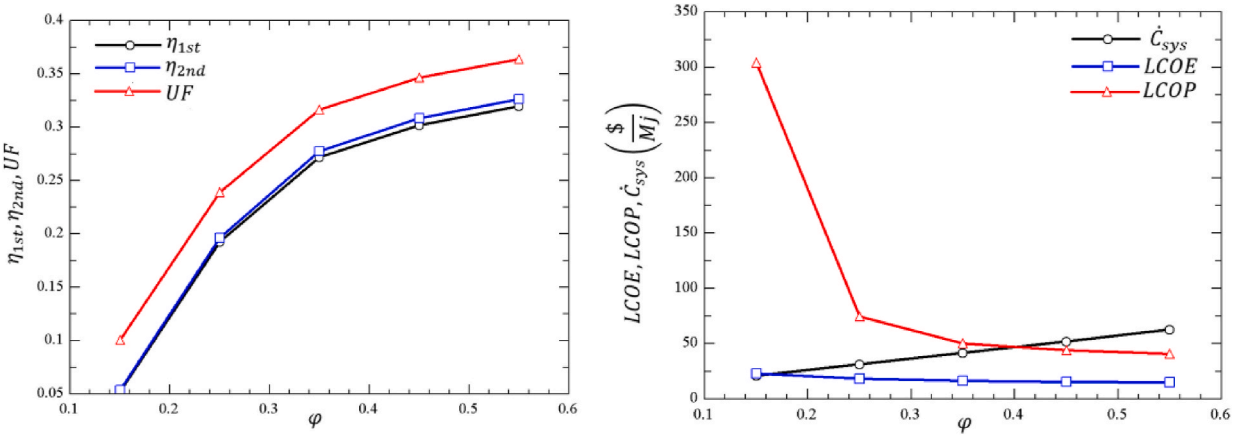

Fig. 3. The impact of Equivalence ratio (ϕ) on objective functions.

3.5.1. *Parameters affecting system performance*

In Fig. 9, the impact of the main parameters on the output responses is depicted. It is important to note that a positive impact implies an increase in the response as the input parameter changes from the lower to the upper limit. This is considered desirable for

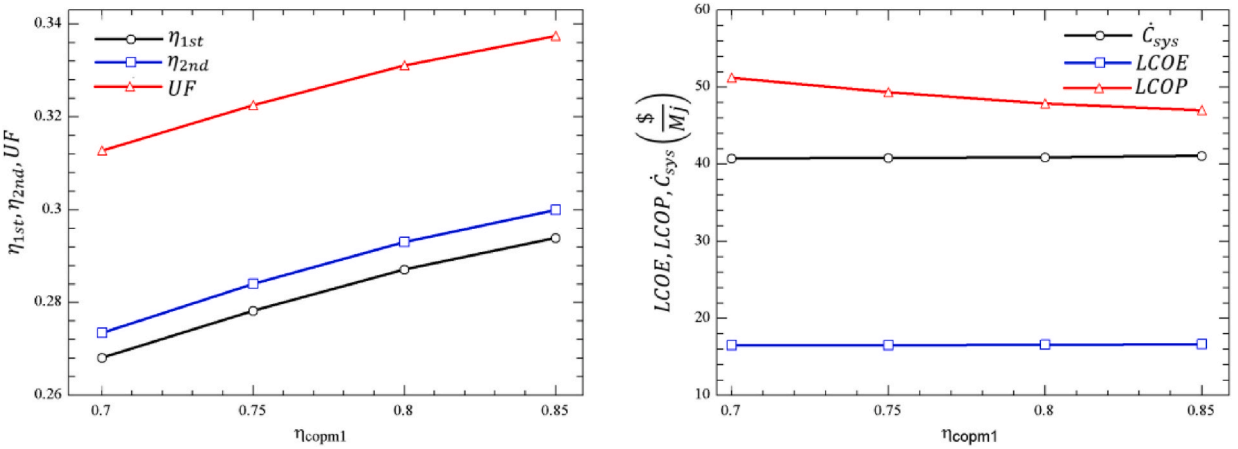

Fig. 4. Effect of the isentropic efficiency of compressor 1 on selected objectives.

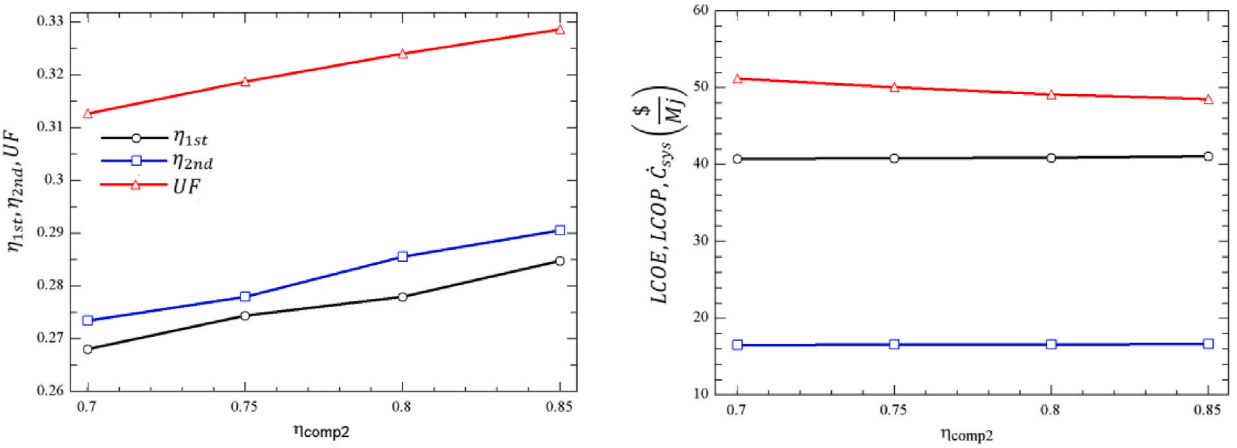

Fig. 5. Effect of the isentropic efficiency of COM 2 on selected objectives.

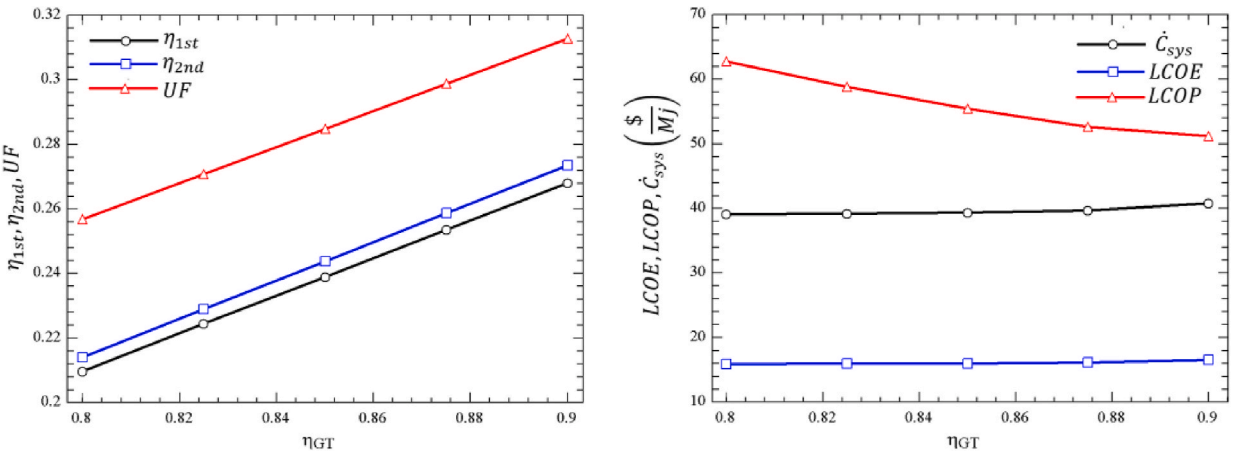

Fig. 6. Effect of gas turbine isentropic efficiency on selected objectives.

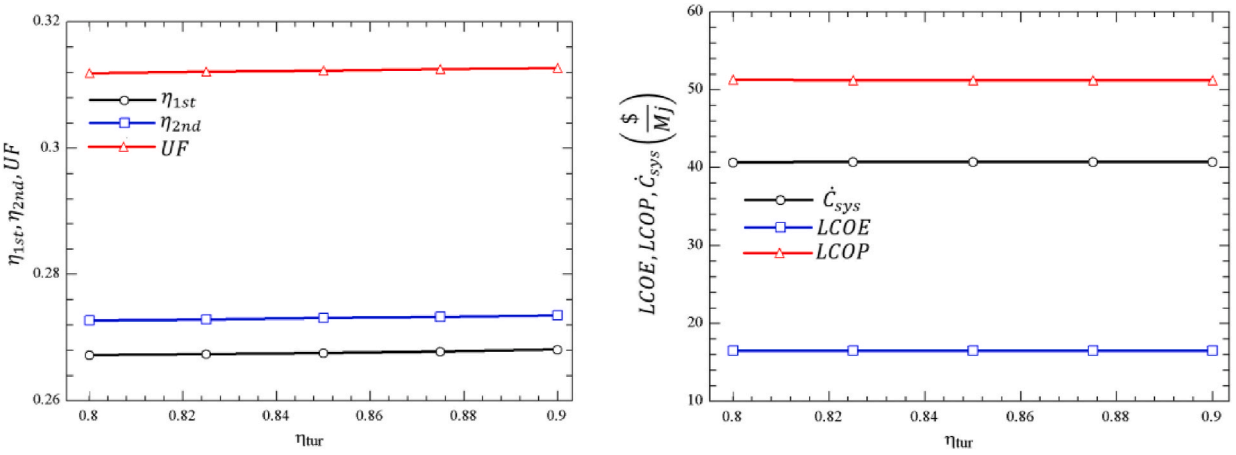

Fig. 7. The effect of isentropic efficiency of TUR on selected objectives.

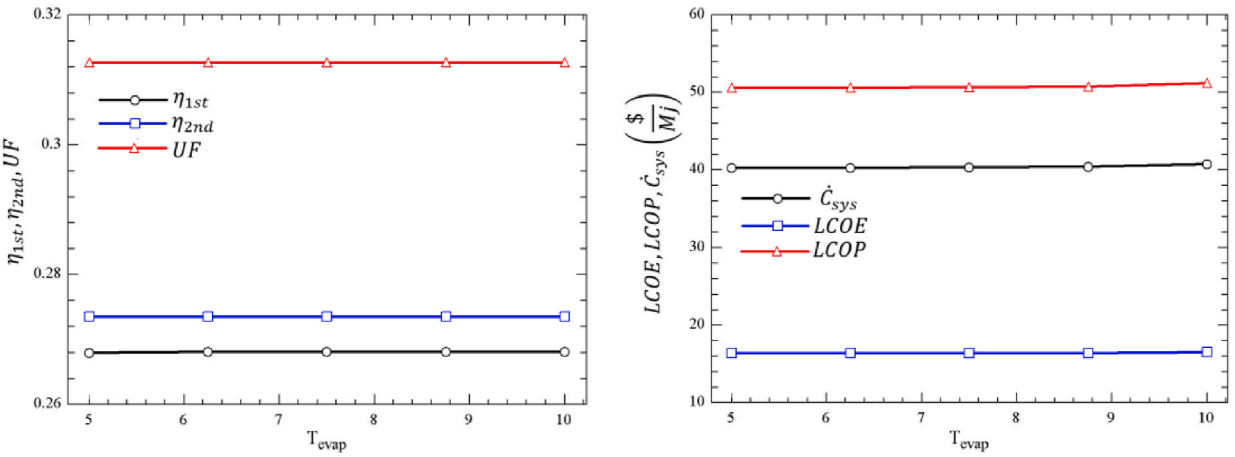

Fig. 8. Effect of evaporator temperature on selected objectives.

Table 15
Input parameters with their upper and lower bounds.

Letter	Factor	Low level	High level
A	φ	0.2	0.55
B	η_{comp1}	0.7	0.825
C	η_{comp2}	0.7	0.85
D	η_{GT}	0.8	0.9
E	η_{tur}	0.8	0.9
F	T_{evap} (K)	278.15	283.15

the first-law efficiency, second-law efficiency, and the utilization factor. Conversely, for the total cost rate, the levelized cost of energy (LCOE), and the levelized cost of power (LCOP), a negative response is considered desirable. The positive and negative effects in the presented graphs are indicated by the slope of the line. A positive slope signifies a positive effect, while a negative slope indicates a negative impact on the response. Additionally, the degree of influence of each parameter on the responses is measured by the angle formed by the graph with the mean line (dotted line). The larger this angle, the more influential the parameter is on the output response.

Now, regarding the first-law efficiency chart of the cycle, it is observed that the parameter with the most significant impact is the air-fuel ratio. By changing the value of ϕ from the lower to the upper limit, the efficiency has increased. After ϕ, the gas turbine isentropic efficiency (η_{GT}) has the most significant impact on energy efficiency. Following that, the isentropic efficiency of compressors 1 and 2 ($\eta_{comp1,2}$), and the efficiency of the Kalina turbine (η_{Tur}), in order, have the most significant impact, resulting in increased system energy efficiency. As evident in the figure, the change in evaporator temperature has no effect on the first-law efficiency of the

Table 16
The results obtained from the simulation for 32 combinatorial states of input parameters.

Num	φ	η_{comp1}	η_{comp2}	η_{GT}	η_{tur}	T_{evap}	η_I	η_{II}	$\dot{C}_{sys}$	UF	LCOE	LCOP
1	0.2	0.825	0.85	0.8	0.8	278.15	0.1384	0.1412	24.41	0.1856	18.6	100.88
2	0.55	0.825	0.7	0.8	0.9	283.15	0.2844	0.2902	61.24	0.323	14.61	44.79
3	0.55	0.7	0.85	0.8	0.9	283.15	0.2801	0.2858	61.39	0.3258	14.66	45.6
4	0.55	0.825	0.85	0.8	0.9	278.15	0.2948	0.3008	61.06	0.3399	14.57	43.09
5	0.55	0.825	0.85	0.9	0.8	278.15	0.3439	0.3509	62.66	0.3869	14.95	37.9
6	0.55	0.825	0.85	0.8	0.8	283.15	0.2941	0.3001	61.47	0.3393	14.67	43.47
7	0.2	0.7	0.85	0.8	0.9	278.15	0.0994	0.1014	24.31	0.1482	18.53	139.88
8	0.2	0.7	0.7	0.9	0.8	283.15	0.1395	0.1424	26.08	0.1866	19.87	106.91
9	0.55	0.7	0.85	0.8	0.8	278.15	0.2794	0.2851	60.83	0.3251	14.54	45.28
10	0.2	0.7	0.7	0.8	0.9	283.15	0.0683	0.0696	24.48	0.1184	18.66	205.16
11	0.55	0.825	0.7	0.8	0.8	278.15	0.2837	0.2895	60.68	0.3293	14.49	44.48
12	0.2	0.7	0.85	0.9	0.9	283.15	0.17	0.1734	26.46	0.2158	20.11	89.03
13	0.2	0.7	0.85	0.8	0.8	283.15	0.0982	0.1002	24.73	0.1471	18.86	144.03
14	0.55	0.7	0.7	0.8	0.9	278.15	0.2686	0.2741	60.6	0.3148	14.48	46.92
15	0.2	0.7	0.7	0.8	0.8	278.15	0.067	0.0684	23.94	0.1172	18.29	204.28
16	0.2	0.825	0.85	0.9	0.9	278.15	0.2078	0.212	26.15	0.2521	19.85	71.98
17	0.2	0.825	0.85	0.8	0.9	283.15	0.1396	0.1425	24.96	0.1868	18.96	102.23
18	0.2	0.825	0.85	0.9	0.8	283.15	0.2066	0.2108	26.57	0.251	20.18	73.56
19	0.2	0.7	0.7	0.9	0.9	278.15	0.1407	0.1436	25.66	0.1878	19.54	104.31
20	0.55	0.825	0.85	0.9	0.9	283.15	0.3445	0.3516	63.23	0.3876	15.06	38.17
21	0.55	0.825	0.7	0.9	0.8	283.15	0.334	0.3409	62.84	0.3775	14.99	39.13
22	0.55	0.825	0.7	0.9	0.9	278.15	0.3347	0.3415	62.44	0.3781	14.88	38.81
23	0.2	0.825	0.7	0.8	0.8	283.15	0.1101	0.1124	24.58	0.1585	18.72	127.68
24	0.55	0.7	0.7	0.8	0.8	283.15	0.268	0.2734	61	0.3142	14.58	47.35
25	0.2	0.825	0.7	0.8	0.9	278.15	0.1113	0.1136	24.16	0.1596	18.39	124.15
26	0.55	0.7	0.85	0.9	0.8	283.15	0.3299	0.3366	62.99	0.3735	15.03	39.72
27	0.2	0.825	0.7	0.9	0.9	283.15	0.1812	0.1849	26.32	0.2267	19.97	83.03
28	0.2	0.825	0.7	0.9	0.8	278.15	0.18	0.1837	25.77	0.2255	19.61	81.86
29	0.55	0.7	0.7	0.9	0.9	283.15	0.3197	0.3262	62.76	0.3637	14.97	40.83
30	0.2	0.7	0.85	0.9	0.8	278.15	0.1688	0.1722	25.91	0.2146	19.75	87.83
31	0.55	0.7	0.85	0.9	0.9	278.15	0.3305	0.3373	62.59	0.3741	14.93	39.38
32	0.55	0.7	0.7	0.9	0.8	278.15	0.319	0.3255	62.2	0.3631	14.85	40.55

cycle. Regarding the second-law efficiency and the system utilization factor, as indicated by the graphs, the influence of the six mentioned parameters on them follows exactly the same trend as the changes in first-law efficiency. The most influential parameter on the total cost rate of the system is the air-fuel ratio (ϕ), and with its increase, the total cost rate ($\dot{C}_{sys}$) also increases. Following ϕ, η_{GT}, T_{EVA}, and η_{Comp2}, in order, contribute to a slight increase in the total cost rate. The air-fuel equivalence ratio (ϕ) shows the most substantial impact on the levelized cost of energy (LCOE). As ϕ increases from the lower bound to the upper, the LCOE decreases. Additionally, an increase in η_{GT} leads to a slight decrease in the levelized cost of energy. The influence of the other parameters is also nearly the same.

ϕ, η_{GT}, η_{Comp1}, and η_{Comp2}, respectively, have the most significant impact on the LCOP. Changing these parameters from the lower bound to the upper results in a reduction in the power production cost. As evident in Fig. 9, the influence of the evaporator temperature and the isentropic efficiency of the Kalina turbine is nearly equal, leading to a marginal increase and decrease, respectively, in the LCOP.

Fig. 10 illustrates the Pareto column chart for the first-law cycle efficiency. In the Pareto chart, parameters are arranged in descending order from top to bottom. The parameter positioned on the left side holds the highest influence on the mentioned response. The blue color signifies a positive impact, while the red color indicates a negative impact for each parameter. Upon closer examination of the chart, it is evident that ϕ, η_{GT}, η_{comp1}, and η_{comp2} exert the most significant influence, leading to an increase in the first-law efficiency. This influence is observed through the interactions between parameters A and B, A and D, and A and C.

The Pareto column chart related to the second-law efficiency and the utilization factor of the system is presented in Figs. 11 and 12, respectively. As evident, the ranking of the influential parameters and the interactions between parameters on the second-law efficiency and the utilization factor is similar to the first-law efficiency.

As mentioned earlier, the air-fuel equivalence ratio is the most important parameter affecting the total cost rate of the system, and with an increase in this parameter, the total cost rate increases. Other parameters do not have a significant impact on the total cost. The Pareto chart related to the total cost rate is presented in Fig. 13.

Fig. 14 illustrates the Pareto chart related to the unit energy production cost. As evident in the figure, the parameter ϕ has the most significant impact on the energy production cost, leading to its reduction. η_{GT} and the interaction between parameters A and D are two additional significant factors. Their variations result in an increase and decrease in the LCOE, respectively.

The Pareto chart related to the power production cost is shown in Fig. 15. As evident, the most influential factors on the LCOP, in order, are related to ϕ, η_{GT}, the interaction between A and D, η_{comp1}, and the interaction between A and B. All of these contribute to a reduction in the LCOP of the system.

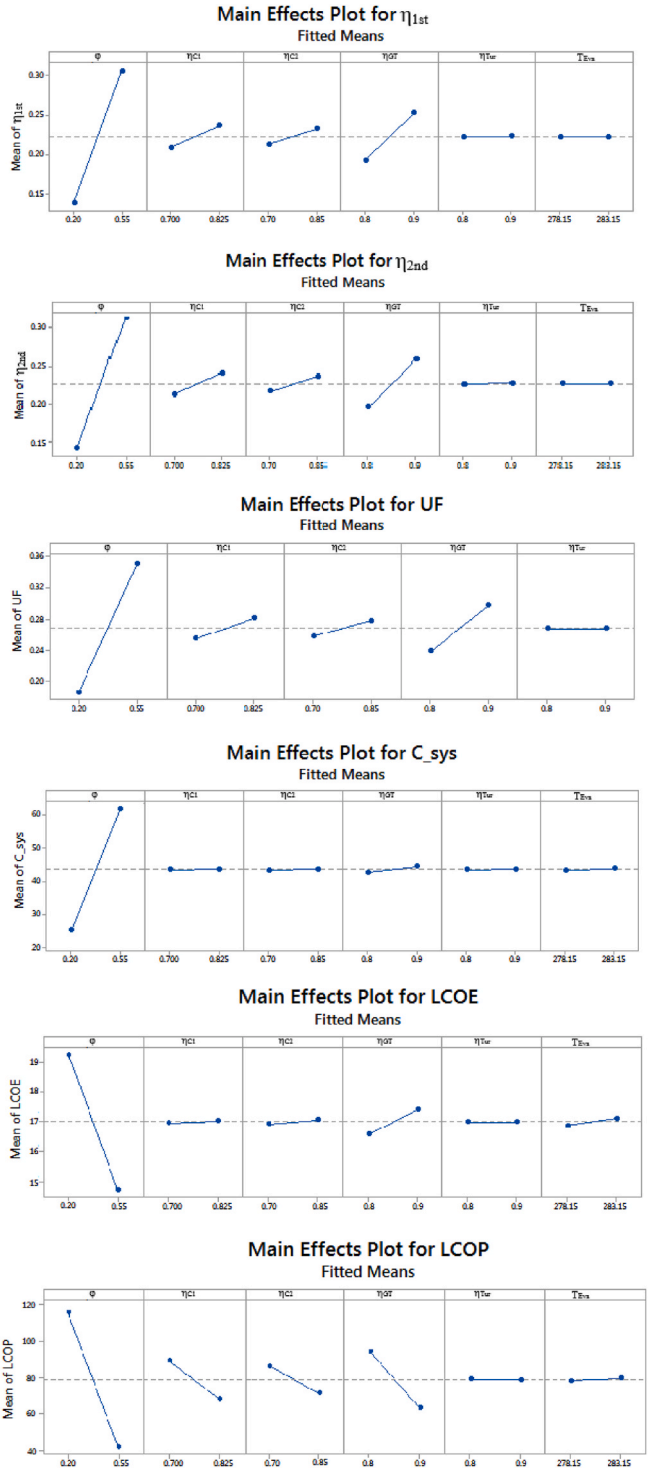

Fig. 9. The influence of the main parameters on the output responses.

3.5.2. Evaluating the effect of parameter interactions on system performance

The Pareto chart reveals the most significant interactions among parameters concerning the system's performance results. However, to comprehend the individual changes of each parameter, interactive effect plots are employed. In these plots, a larger angle between the upper and lower limit lines of a parameter signifies that its interactive effect with another parameter has the most

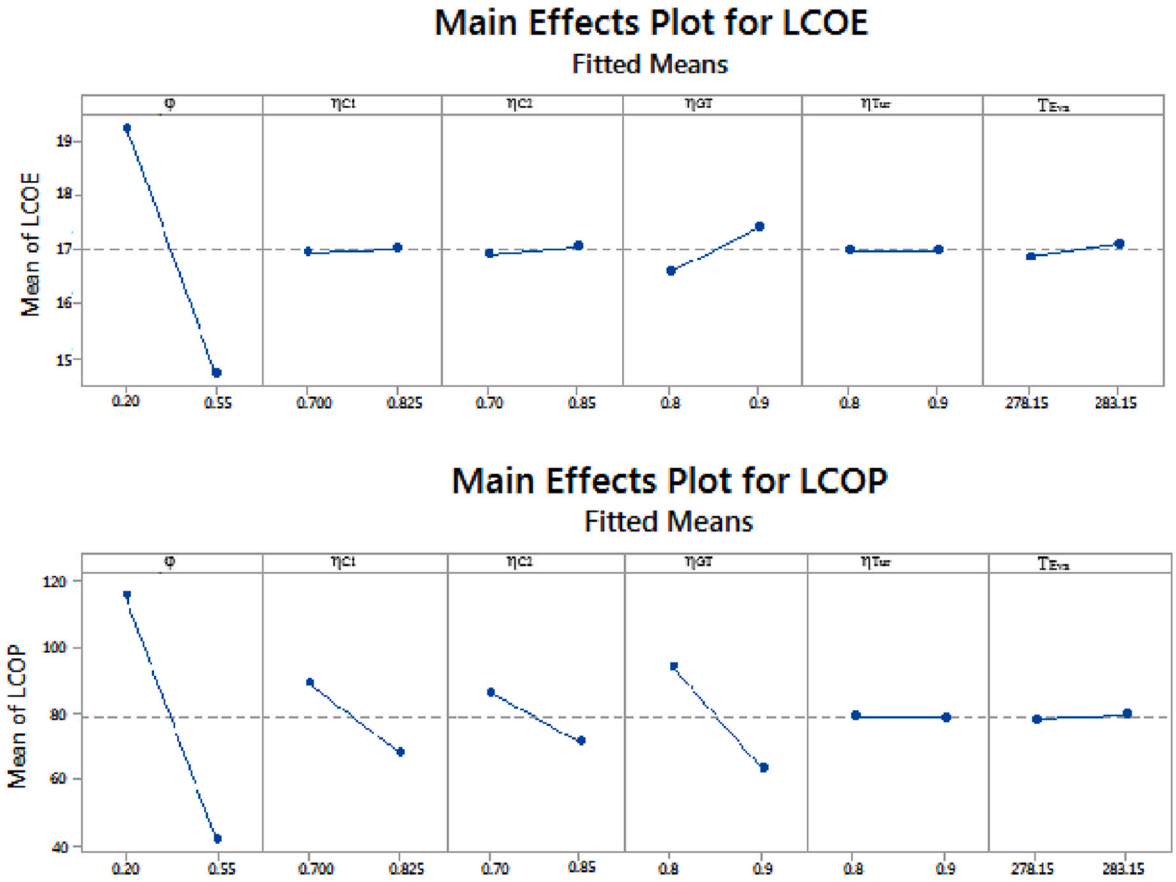

Fig. 9. (*continued*).

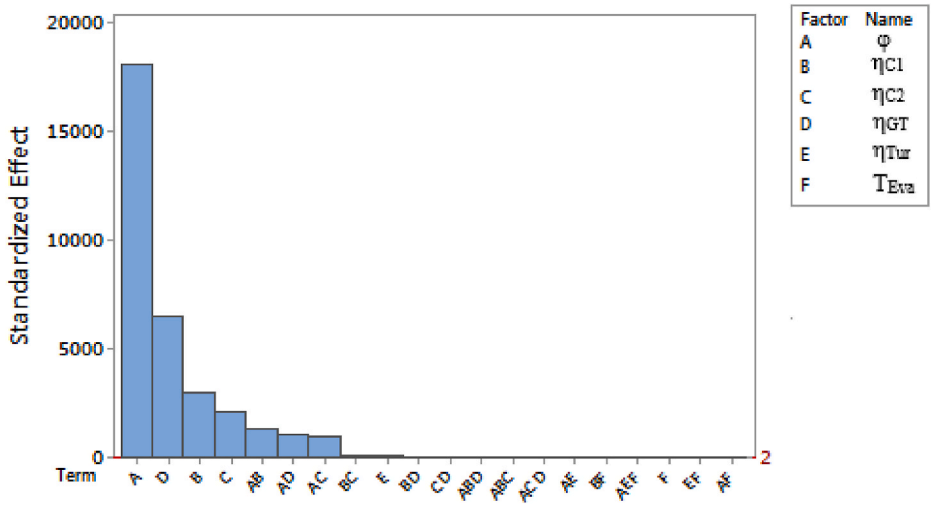

Fig. 10. The Pareto chart of the first-law efficiency of the system.

substantial impact on the response.

Figs. 16 and 17 depict the influence of parameter interactions on the first and second-law efficiency of the system, respectively. These figures not only reveal the order of importance of interactions but also illustrate how parameters change. As evident in both figures, to optimize both first and second-law efficiencies in the interaction between ϕ and η_{comp1}, both parameters must be at their upper bounds. Similarly, for interactions between ϕ, η_{GT}, and ϕ, η_{comp2} to achieve maximum efficiency, parameter values must be at

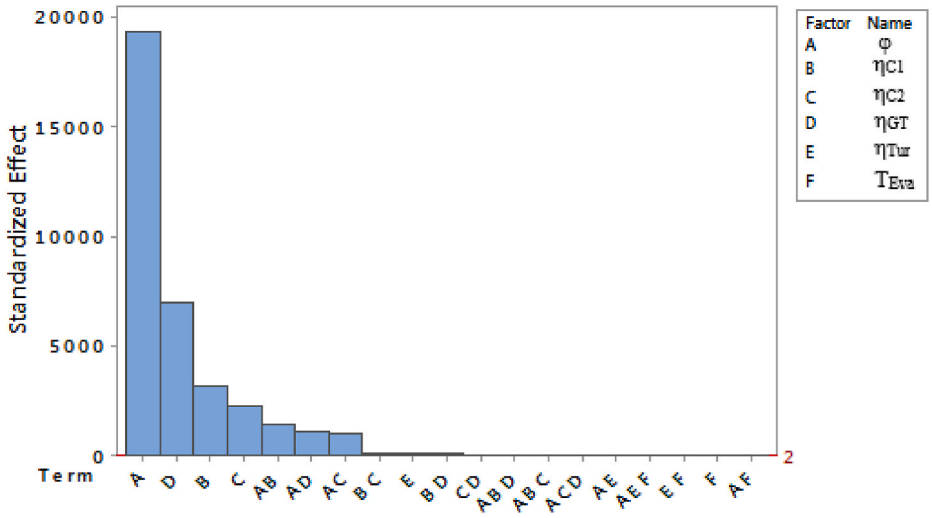

Fig. 11. The Pareto chart of the second-law efficiency of the system.

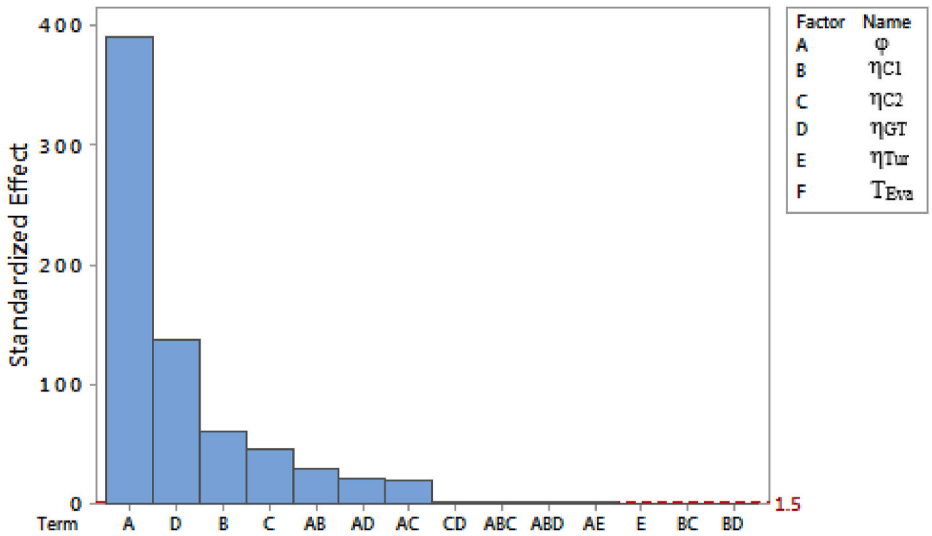

Fig. 12. The Pareto chart of the utilization factor.

their upper bounds.

Fig. 18 also illustrates the impact of parameter interactions on the utilization factor. As observed in the figure, the manner in which the interaction between parameters affects the utilization factor is similar to how parameter interactions affect the first and second-law efficiencies.

The Pareto chart related to the total cost rate, as shown in Fig. 19, indicates that the interaction between parameters has an insignificant impact on the total cost rate. According to the figure, when the air-fuel equivalence ratio is at its lower limit, irrespective of other parameters, the total cost rate decreases.

The influence of parameter interactions on the levelized cost of energy (LCOE) is depicted in Fig. 20. Clearly, the interaction between ϕ and η_{GT} has the most substantial effect. When η_{GT} is at its lower limit and ϕ is at its upper limit, the cost of energy production is minimized. In the reciprocal influence of ϕ and T_{EVA}, if T_{EVA} is at its lower limit and ϕ is at its upper limit, the LCOE.

As demonstrated in Fig. 21, the interaction between ϕ and η_{GT} has the most significant effect on the LCOP. The LCOP is minimized when both parameters are at their upper limits. The chart also indicates that when parameters ϕ and η_{comp1}, as well as ϕ and η_{comp2}, are at their upper limits, the unit power production cost decreases.

Table 17 provides a detailed comparison of the present work with the studies conducted by Wang et al. [62], Kalan et al. [24], and Ebrahimi-Moghaddam et al. [63], highlighting the similarities, differences, and advancements made in this study relative to the referenced works.

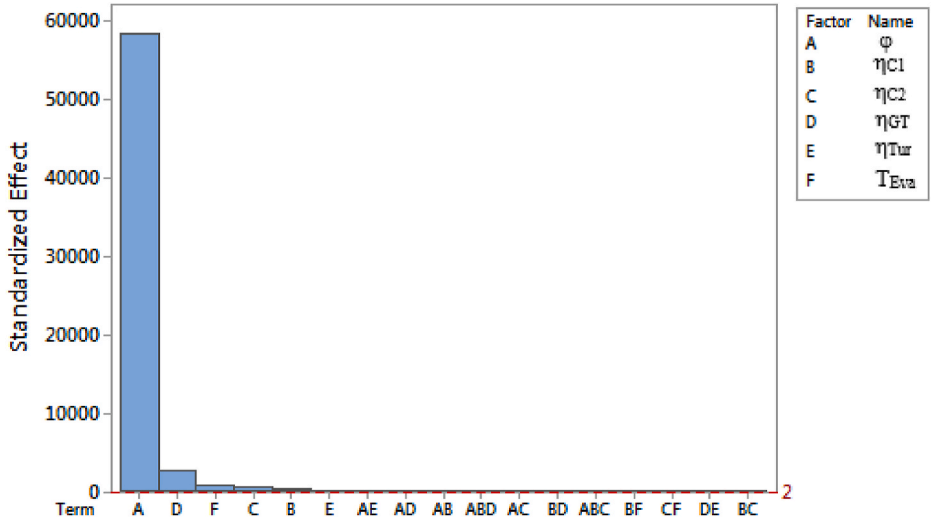

Fig. 13. The Pareto chart of the total cost rate of the system.

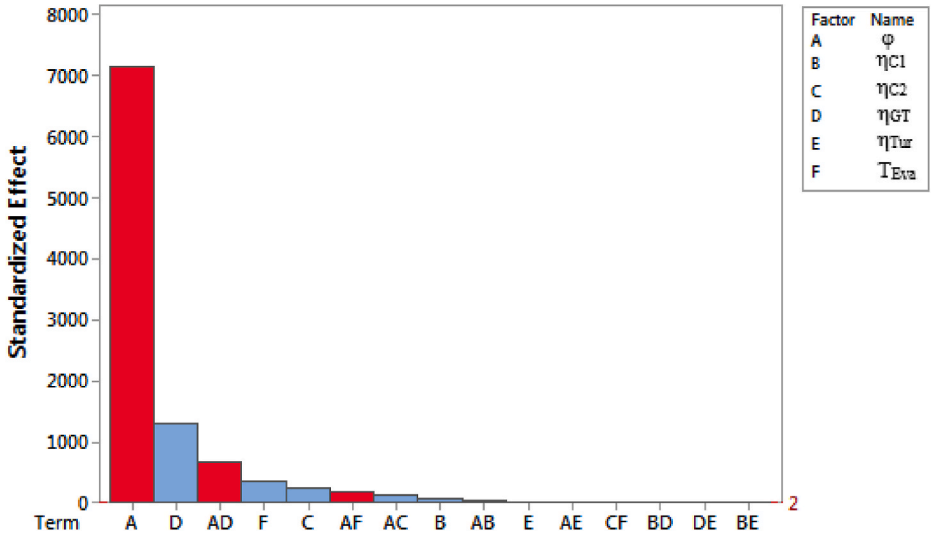

Fig. 14. The Pareto chart of the levelized cost of energy.

4. Conclusion

In this study, a cogeneration power, cooling, and heating system based on the combined cycle of gas turbine power generation, Kalina power generation cycle, and refrigeration cycle has been designed. Initially, the data obtained from the simulation of these cycles were validated against results presented in the literature. Subsequently, the integrated cycle was analyzed in terms of energy, exergy, and exergo-economic perspectives. The cycle was then evaluated using parametric study and Design of Experiments (DOE) methods. The influence of various parameters on the system's performance results was assessed.

The most important results that can be obtained from the present study are as follows:

- In the baseline design scenario, the system has power generation, cooling capacity, and heating capacity of 0.8, 0.4, and 1.2 MW, respectively. Additionally, the Levelized Cost of Energy (LCOE) and Levelized Cost of Power (LCOP) are 16.53 $/MWh and $51.19 $/MWh, respectively.
- The present system comprises three subsystems: Brayton, absorption refrigeration, and Kalina cycles. The highest exergy destruction occurs in the following order: Brayton, Kalina, and then absorption refrigeration cycles. Within the system components, the combustion chamber and HX2 exhibit the highest exergy destruction and the lowest exergy efficiency are related to absorber

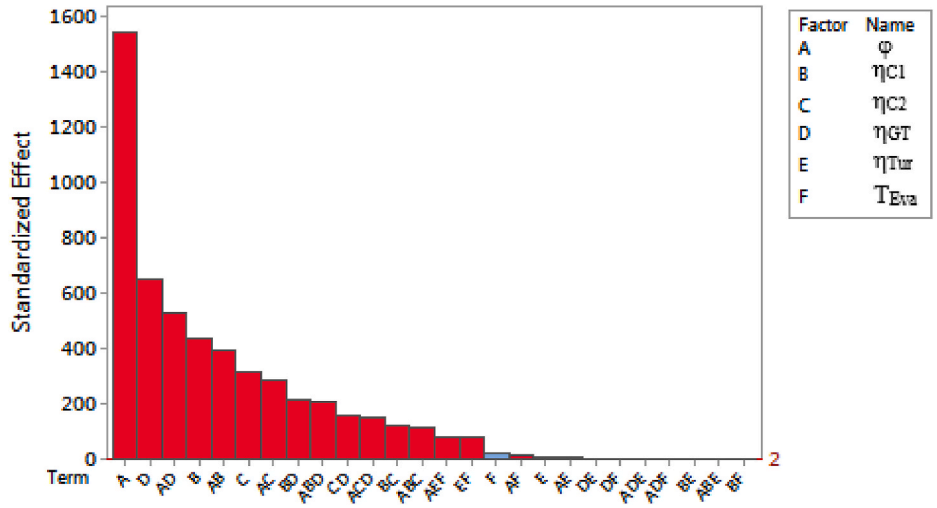

Fig. 15. The Pareto chart of the levelized cost of power.

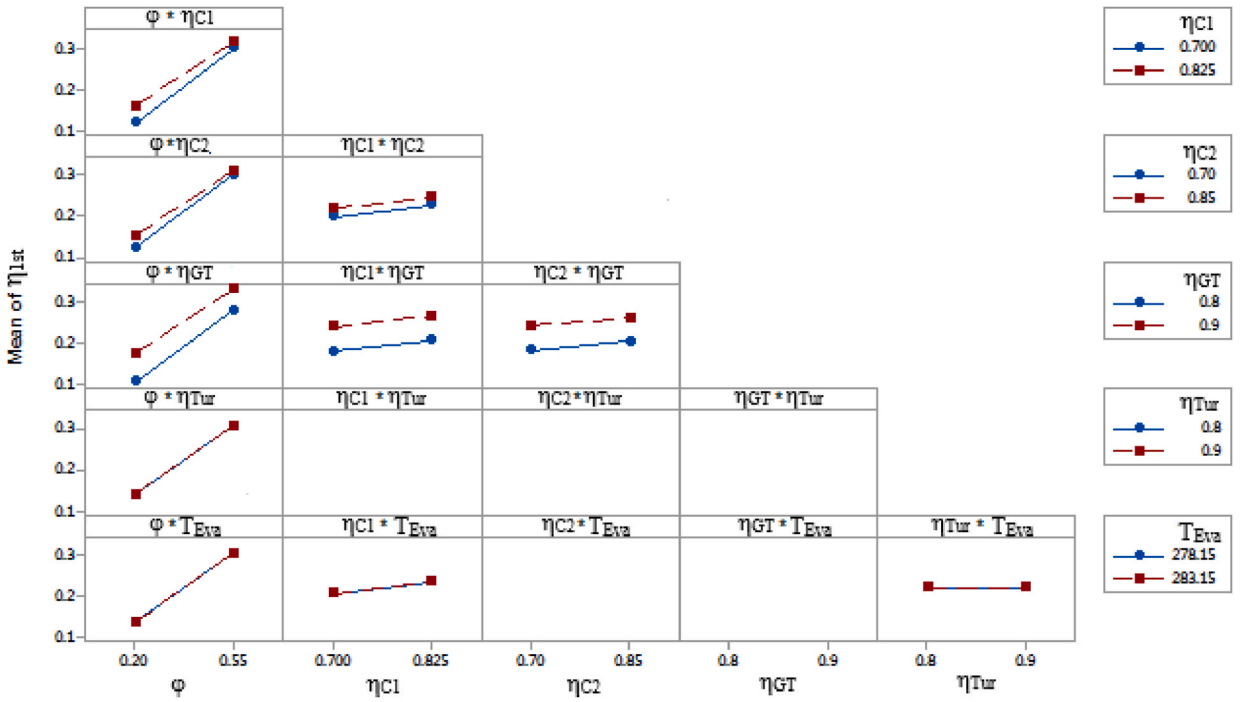

Fig. 16. Chart of the interaction effect of parameters on the first-law efficiency of the system.

and HX2, respectively. Additionally, the combustion chamber and HX2 are associated with the highest total investment and exergy destruction costs, respectively.

- The air-fuel equivalence ratio is the most influential parameter affecting the system's performance. As this ratio increases, the values associated with the first and second-law efficiencies of the system, as well as the Utilization Factor (UF), increase. Moreover, the Levelized Cost of Energy (LCOE) and Levelized Cost of Power (LCOP) significantly decrease. However, due to the heightened fuel consumption, the total cost rate of the system($\dot{C}_{sys}$) also increases.
- Regarding the first-law efficiency, second-law efficiency, and the utilization factor, after the parameters ϕ, η_{comp1}, η_{GT}, and η_{comp2}, the most significant influence, respectively, is related to the interaction between the parameters ϕ, η_{comp1}, and ϕ, η_{GT}. In such a case, if these parameters are at their upper limits, the values of first and second-law efficiencies and the utilization factor are maximized.
- The interaction between ϕ and η_{GT} is the most influential interaction affecting the levelized cost of energy (LCOE) of the system. The minimum LCOE of the system occurs when ϕ is at its upper limit, and η_{GT} is at its lower limit.

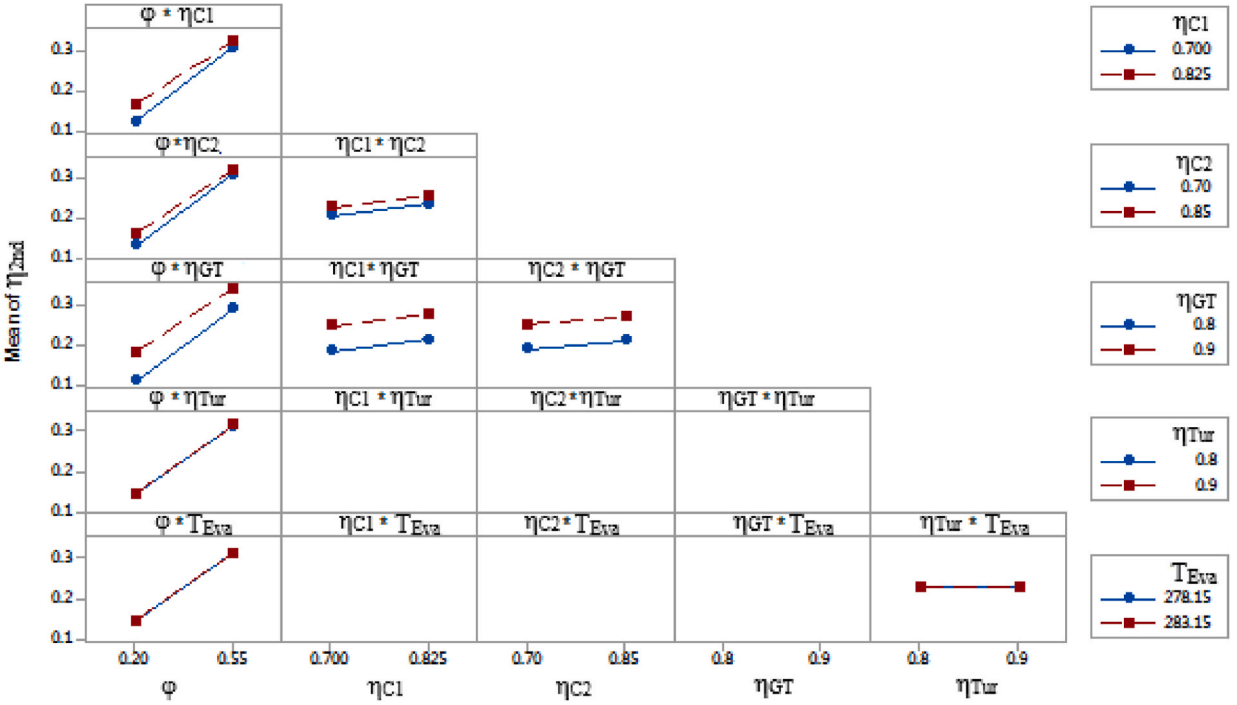

Fig. 17. Chart of the Interaction Effect of Parameters on the second-Law Efficiency of the System.

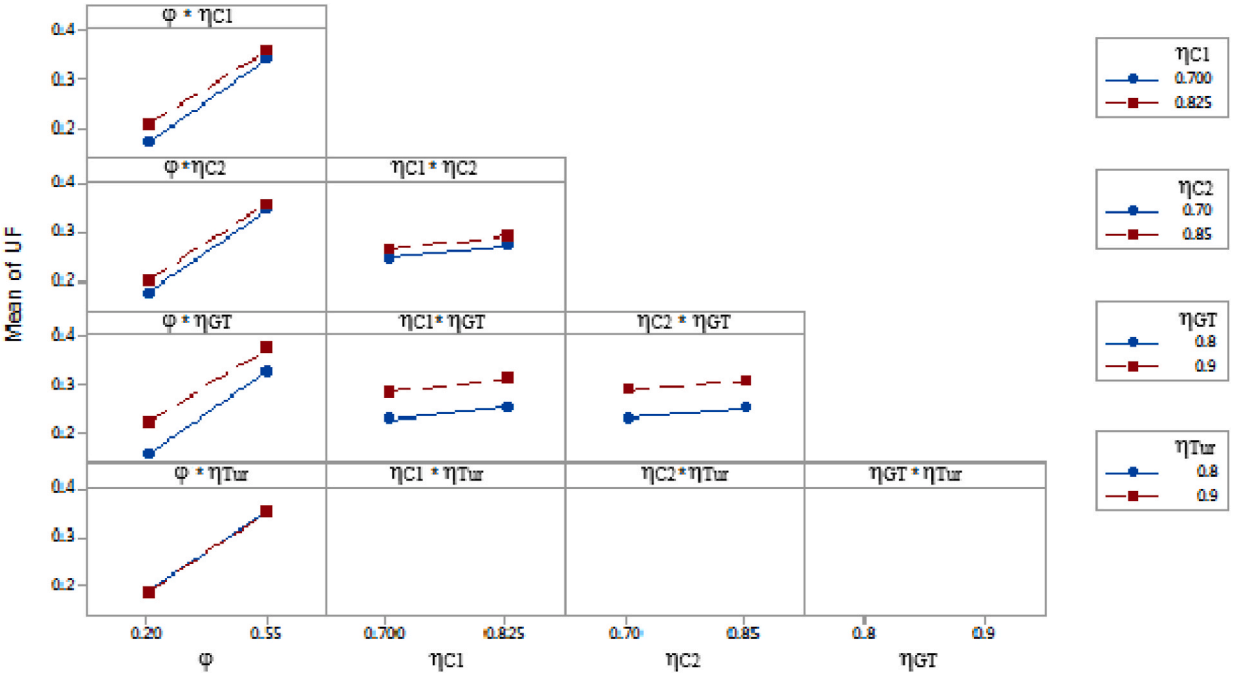

Fig. 18. Pareto chart of the Interaction Effect of Parameters on the utilization factor of the System.

- The most influential interaction affecting the levelized cost of power (LCOP) of the system is the interaction between ϕ and η_{GT}. When their values are at their maximum, the LCOP of the system decreases.
- The interaction between parameters does not have a significant effect on the total cost rate of the system.

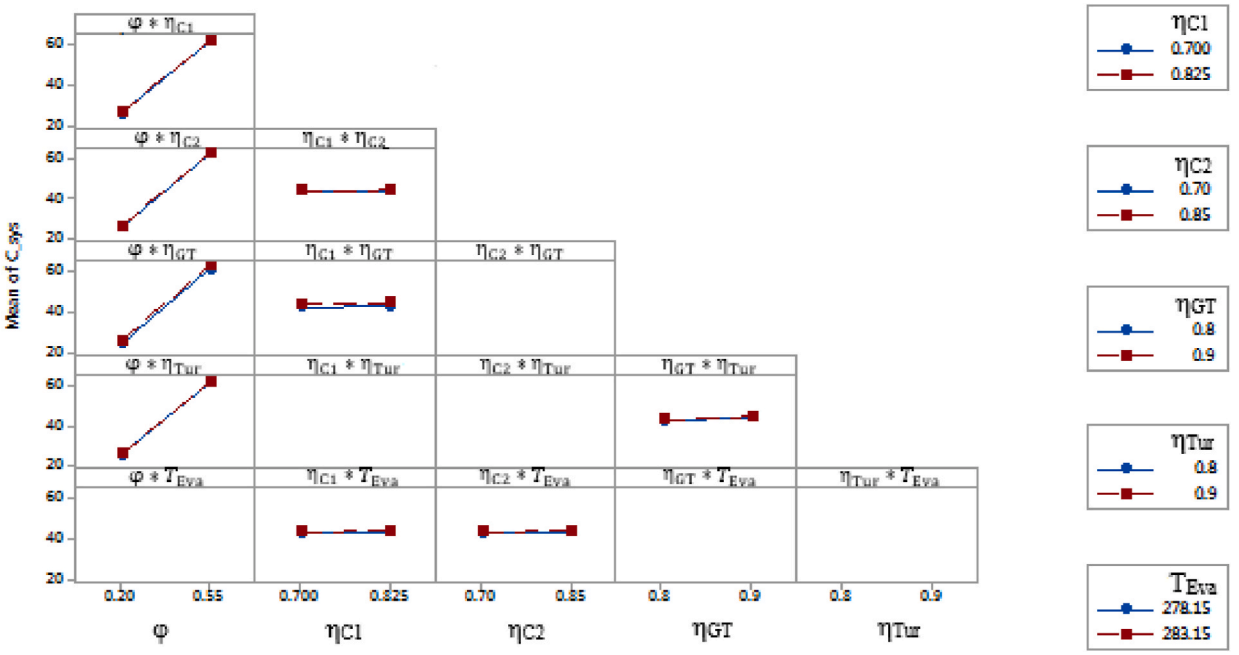

Fig. 19. Pareto chart of the Interaction Effect of Parameters on the Total System Cost rate.

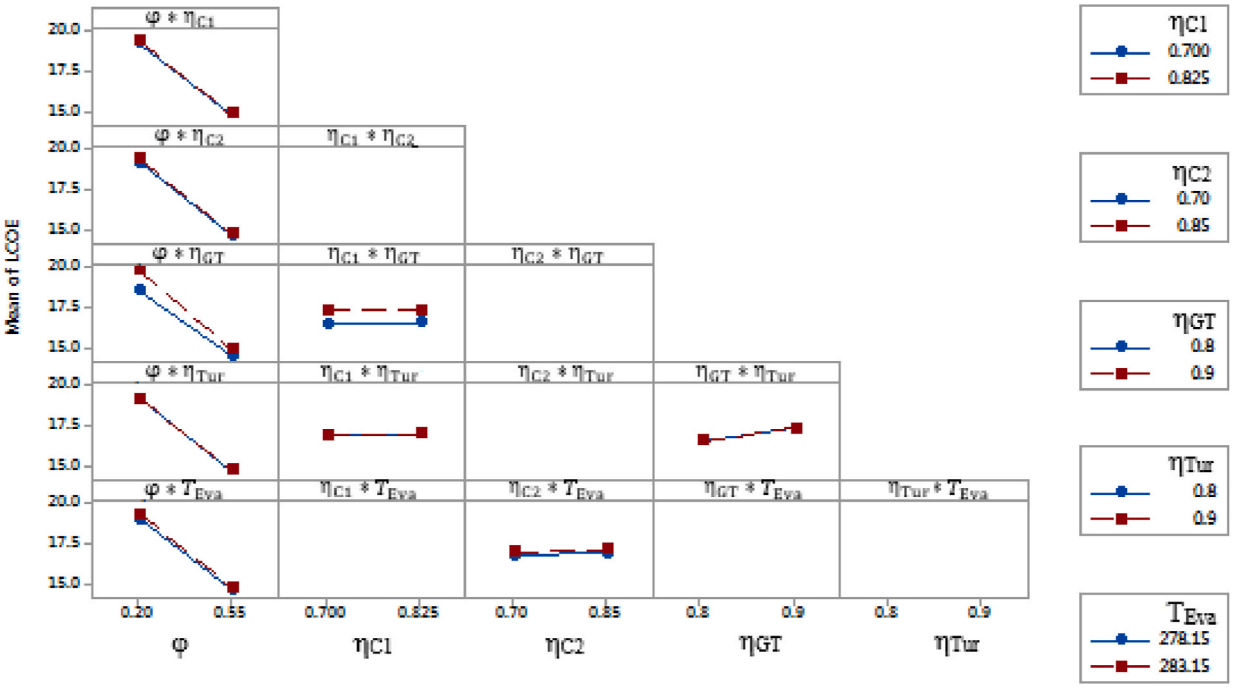

Fig. 20. Pareto chart of the Interaction Effect of Parameters on the LCOE.

CRediT authorship contribution statement

Reza Hajipour: Validation, Project administration, Methodology, Formal analysis. **Elaheh Neshat:** Writing – review & editing, Validation, Supervision, Methodology. **Ali Shokri Kalan:** Writing – original draft, Investigation.

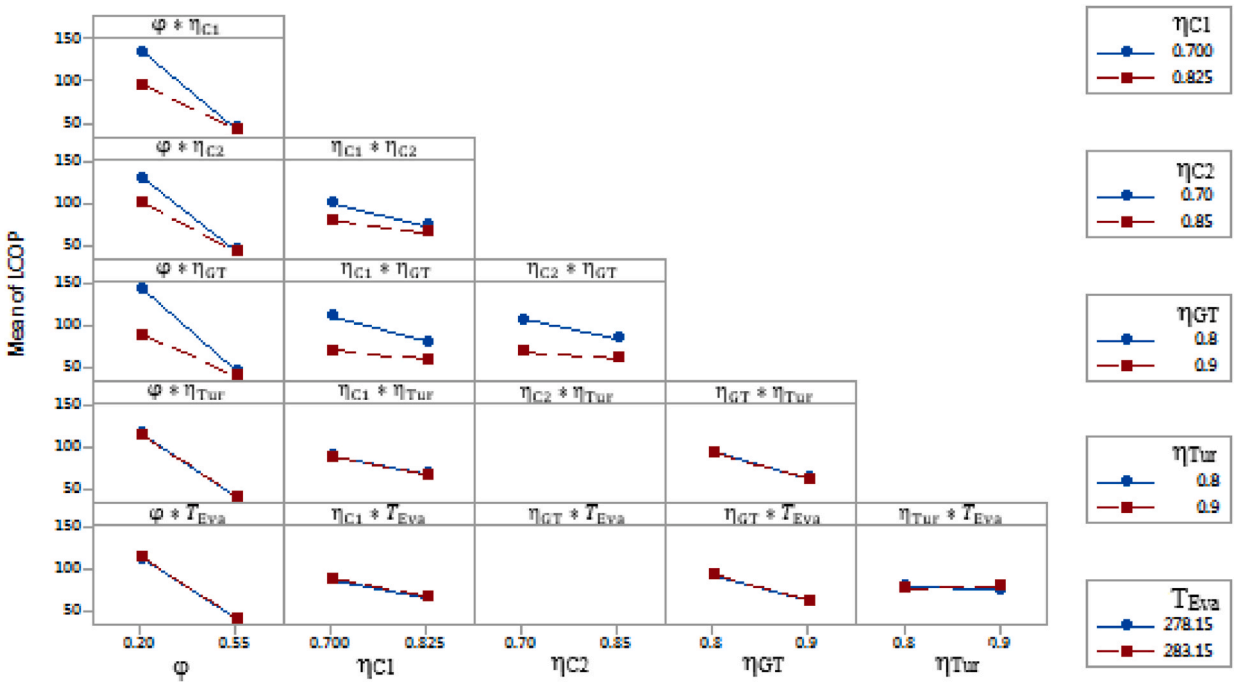

Fig. 21. Pareto chart of the Interaction Effect of Parameters on the LCOP.

Table 17
Comparison of the present work with referenced studies [reference].

Parameters	Present work	[24]	[62]	[63]
Power production rate (kW)	1019.776	423.47	–	1050
Heating capacity (kW)	1292	–	–	836.4
Energy Efficiency (%)	34.3	28.3	77.17	69.37
Exergy Efficiency (%)	34.95	54.37	38.94	37.95

Declaration of competing interest

The authors declare that they have no known competing financial interests or personal relationships that could have appeared to influence the work reported in this paper.

Acknowledgements

The authors would like to thank the INSF for the support of this study [Grant number: 98018500].

Data availability

Data will be made available on request.

References

[1] M. Ebadollahi, M. Amidpour, O. Pourali, H. Ghaebi, Development of a novel flexible multigeneration energy system for meeting the energy needs of remote areas, Renew. Energy 198 (2022) 1224–1242.
[2] X. Sun, Y. Zhuang, L. Liu, Y. Dong, L. Zhang, J. Du, Multi-objective optimization of heat exchange network and thermodynamic cycles integrated system for cooling and power cogeneration, Appl. Energy 321 (2022) 119366.
[3] S.F. Ahmadi, A. Minaei, M. Ebadollahi, H. Ghaebi, M.H. Shahrivar, Energy management and reducing the environmental impacts of industrial flare gases using a new trigeneration energy system, Process Saf. Environ. Prot. 177 (2023) 1129–1141.
[4] A. Ebrahimi-Moghadam, M. Farzaneh-Gord, Optimal operation of a multi-generation district energy hub based on electrical, heating, and cooling demands and hydrogen production, Appl. Energy 309 (2022) 118453.
[5] T. Zhang, H. Zhao, H. Du, H. Wang, Thermodynamic performance study of a novel cogeneration system combining solid oxide fuel cell, gas turbine, organic Rankine cycle with compressed air energy storage, Energy Convers. Manag. 249 (2021) 114837.
[6] W. Tianliang, T. Hong, Thermodynamic and exergoeconomic analysis of an innovative cogeneration of power and freshwater based on gas turbine cycle, Energy 285 (2023) 129454.

[7] Y.A. de Oliveira Chaves, M. Val Springer, R.A.M. Boloy, O.M. de Castro Ferreira Soares, J.G.F. Madeira, Performance study of a microturbine system for cogeneration application using biogas from manipueira, BioEnergy Research 13 (2020) 659–667.
[8] M. Panowski, R. Zarzycki, R. Kobyłecki, Conversion of steam power plant into cogeneration unit - case study, Energy 231 (2021) 120872.
[9] Y. Koc, O. Kose, H. Yagli, Exergy analysis of a natural gas fuelled gas turbine based cogeneration cycle, Int. J. Exergy 30 (2019) 103–125.
[10] S. Khosravi, R.K. Saray, E. Neshat, A. Arabkoohsar, Towards an environmentally friendly power and hydrogen co-generation system: integration of solar-based sorption enhanced gasification with in-situ CO2 capture and liquefaction process, Chemosphere 343 (2023) 140226.
[11] M. Świerzewski, J. Kalina, Optimisation of biomass-fired cogeneration plants using ORC technology, Renew. Energy 159 (2020) 195–214.
[12] A. Karimi, A. Gimelli, R. Iossa, M. Muccillo, Techno-economic simulation and sensitivity analysis of modular cogeneration with organic rankine cycle and battery energy storage system for enhanced energy performance, Energy 295 (2024) 131021.
[13] Z. Liu, Z. Liu, X. Cao, H. Li, X. Yang, Self-condensing transcritical CO2 cogeneration system with extraction turbine and ejector refrigeration cycle: a techno-economic assessment study, Energy 208 (2020) 118391.
[14] S. Mohtaram, M. Omidi, J. Lin, H. Sun, W. Chen, Exergy analysis of a multi mixture working fluid absorption refrigeration cycle, Case Stud. Therm. Eng. 15 (2019) 100540.
[15] M. Aghabalazadeh, E. Neshat, Proposal and optimization of a novel biomass-based tri-generation system using energy, exergy and exergoeconomic analyses and design of experiments method, Energy 288 (2024) 129723.
[16] M. Ebadollahi, B. Shahbazi, H. Ghaebi, Efficiency and flexibility enhancement of nanofluid-based hybrid solar desalination system equipped with thermoelectric generator for eco-friendly freshwater and power cogeneration, Process Saf. Environ. Prot. 190 (2024) 108–122.
[17] A. Pirmohamadi, H. Ghaebi, B.M. Ziapour, M. Ebadollahi, Exergoeconomic analysis of a novel hybrid system by integrating the Kalina and heat pump cycles with a nitrogen closed Brayton system, Energy Rep. 7 (2021) 546–564.
[18] A. Jamali, P. Ahmadi, M.N.M. Jaafar, Optimization of a novel carbon dioxide cogeneration system using artificial neural network and multi-objective genetic algorithm, Appl. Therm. Eng. 64 (2014) 293–306.
[19] P. Ahmadi, I. Dincer, Exergoenvironmental analysis and optimization of a cogeneration plant system using Multimodal Genetic Algorithm (MGA), Energy 35 (2010) 5161–5172.
[20] A.D. Zare, R.K. Saray, S. Mirmasoumi, K. Bahlouli, Optimization strategies for mixing ratio of biogas and natural gas co-firing in a cogeneration of heat and power cycle, Energy 181 (2019) 635–644.
[21] M. Mehregan, M. Abbasi, S.M. Hashemian, Technical, economic and environmental analyses of combined heat and power (CHP) system with hybrid prime mover and optimization using genetic algorithm, Sustain. Energy Technol. Assessments 49 (2022) 101697.
[22] P. Kazemiani-Najafabadi, E.A. Rad, Multi-objective optimization of a novel offshore CHP plant based on a 3E analysis, Energy 224 (2021) 120135.
[23] Y. Yuan, L. Chen, X. Lyu, W. Ning, W. Liu, W.-Q. Tao, Modeling and optimization of a residential PEMFC-based CHP system under different operating modes, Appl. Energy 353 (2024) 122066.
[24] A.S. Kalan, H. Ghiasirad, R.K. Saray, S. Mirmasoumi, Thermo-economic evaluation and multi-objective optimization of a waste heat driven combined cooling and power system based on a modified Kalina cycle, Energy Convers. Manag. 247 (2021) 114723.
[25] A. Farajollahi, M. Baharvand, H.R. Takleh, Modeling and optimization of hybrid geothermal-solar energy plant using coupled artificial neural network and genetic algorithm, Process Saf. Environ. Prot. 186 (2024) 348–360.
[26] J. Huang, A.M. Abed, S.M. Eldin, Y. Aryanfar, J.L. García Alcaraz, Exergy analyses and optimization of a single flash geothermal power plant combined with a trans-critical CO2 cycle using genetic algorithm and Nelder–Mead simplex method, Geoth. Energy 11 (2023) 4.
[27] K. Alhamad, Y. Alkhezi, Hybrid genetic algorithm and tabu search for solving preventive maintenance scheduling problem for cogeneration plants, Mathematics 12 (2024) 1881.
[28] S. Khosravi, D. Roy, R.K. Saray, E. Neshat, A. Arabkoohsar, Techno-economic analysis, emergy assessment, and optimization using response surface methodology of a solar and biomass-based co-generation system, Energy Convers. Manag. 307 (2024) 118376.
[29] S. Azizi, H. Shakibi, A. Shokri, A. Chitsaz, M. Yari, Multi-aspect analysis and RSM-based optimization of a novel dual-source electricity and cooling cogeneration system, Appl. Energy 332 (2023) 120487.
[30] A. Habibollahzade, Z.K. Mehrabadi, C.N. Markides, Comparative thermoeconomic analyses and multi-objective particle swarm optimization of geothermal combined cooling and power systems, Energy Convers. Manag. 234 (2021) 113921.
[31] X. Lv, Y. Lv, Y. Zhu, Multi-variable study and MOPSO-based multi-objective optimization of a novel cogeneration plant using biomass fuel and geothermal energy: a complementary hybrid design, Energy 270 (2023) 126921.
[32] N. Nazari, S. Mousavi, S. Mirjalili, Exergo-economic analysis and multi-objective multi-verse optimization of a solar/biomass-based trigeneration system using externally-fired gas turbine, organic Rankine cycle and absorption refrigeration cycle, Appl. Therm. Eng. 191 (2021) 116889.
[33] G. Zhang, H. Li, C. Xiao, B. Sobhani, Multi-aspect analysis and multi-objective optimization of a novel biomass-driven heat and power cogeneration system; utilization of grey wolf optimizer, J. Clean. Prod. 355 (2022) 131442.
[34] H.U.R. Habib, S. Wang, A. Waqar, B.S. Farhan, K.M. Kotb, Y.-S. Kim, Combined heat and power units sizing and energy cost optimization of a residential building by using an artificial bee colony algorithm, IEEE Access 8 (2020) 218289–218303.
[35] J. Antony, Design of Experiments for Engineers and Scientists, Elsevier, 2023.
[36] O.A. Mohamed, S.H. Masood, J.L. Bhowmik, Optimization of fused deposition modeling process parameters: a review of current research and future prospects, Advances in manufacturing. 3 (2015) 42–53.
[37] M. Nazemian, E. Neshat, R.K. Saray, Effects of piston geometry and injection strategy on the capacity improvement of waste heat recovery from RCCI engines utilizing DOE method, Appl. Therm. Eng. 152 (2019) 52–66.
[38] J. Pátek, J. Klomfar, A computationally effective formulation of the thermodynamic properties of LiBr–H2O solutions from 273 to 500 K over full composition range, Int. J. Refrig. 29 (2006) 566–578.
[39] M. Wang, A. Manera, S. Qiu, G. Su, Ammonia-water mixture property code (AWProC) development, verification and Kalina cycle design for nuclear power plant, Prog. Nucl. Energy 91 (2016) 26–37.
[40] B.J. McBride, NASA Glenn Coefficients for Calculating Thermodynamic Properties of Individual Species, National Aeronautics and Space Administration, John H. Glenn Research Center, 2002.
[41] M. Ebadollahi, H. Rostamzadeh, O. Pourali, H. Ghaebi, M. Amidpour, Close supercritical versus inverse Brayton cycles for power supply, using waste of a biogas-driven open Brayton cycle, J. Energy Resour. Technol. 143 (2021) 092102.
[42] V. Zare, S.S. Mahmoudi, M. Yari, M. Amidpour, Thermoeconomic analysis and optimization of an ammonia–water power/cooling cogeneration cycle, Energy 47 (2012) 271–283.
[43] P. Ahmadi, I. Dincer, M.A. Rosen, Exergy, exergoeconomic and environmental analyses and evolutionary algorithm based multi-objective optimization of combined cycle power plants, Energy 36 (2011) 5886–5898.
[44] A. Bejan, G. Tsatsaronis, M. Moran, M.J. Moran, Thermal Design and Optimization, John Wiley & Sons, 1996.
[45] K. Li, Applied Thermodynamics: Availability Method and Energy Conversion, Routledge, 2018.
[46] A. Lazzaretto, G. Tsatsaronis, SPECO: a systematic and general methodology for calculating efficiencies and costs in thermal systems, Energy 31 (2006) 1257–1289.
[47] A. Ebrahimi-Moghadam, A.J. Moghadam, M. Farzaneh-Gord, Comprehensive techno-economic and environmental sensitivity analysis and multi-objective optimization of a novel heat and power system for natural gas city gate stations, J. Clean. Prod. 262 (2020) 121261.
[48] M. Khaljani, R.K. Saray, K. Bahlouli, Comprehensive analysis of energy, exergy and exergo-economic of cogeneration of heat and power in a combined gas turbine and organic Rankine cycle, Energy Convers. Manag. 97 (2015) 154–165.
[49] T. McMahon, Inflationdata.com [Online]. Available: https://inflationdata.com/Inflation/Inflation_Rate/HistoricalInflation.aspx. (Accessed 19 January 2024).

[50] S. Mahmoudi, A. Pourreza, A. Akbari, M. Yari, Exergoeconomic evaluation and optimization of a novel combined augmented Kalina cycle/gas turbine-modular helium reactor, Appl. Therm. Eng. 109 (2016) 109–120.
[51] R. Misra, P. Sahoo, S. Sahoo, A. Gupta, Thermoeconomic optimization of a single effect water/LiBr vapour absorption refrigeration system, Int. J. Refrig. 26 (2003) 158–169.
[52] J. Rashidi, P. Ifaei, I.J. Esfahani, A. Ataei, C.K. Yoo, Thermodynamic and economic studies of two new high efficient power-cooling cogeneration systems based on Kalina and absorption refrigeration cycles, Energy Convers. Manag. 127 (2016) 170–186.
[53] A. Modi, F. Haglind, Performance analysis of a Kalina cycle for a central receiver solar thermal power plant with direct steam generation, Appl. Therm.Eng. 65 (1–2) (2014) 201–208.
[54] E. Gholamian, V. Zare, A comparative thermodynamic investigation with environmental analysis of SOFC waste heat to power conversion employing Kalina and Organic Rankine Cycles, Energy Convers. Manag. 117 (2016) 150–161.
[55] U.S. Energy Information Administration, ."S. Energy Information Administration (EIA)." [Online]. Available: https://www.eia.gov/.
[56] C. Beatrice, P. Napolitano, C. Guido, Injection parameter optimization by DoE of a light-duty diesel engine fed by Bio-ethanol/RME/diesel blend, Appl. Energy 113 (2014) 373–384.
[57] J. Li, W.M. Yang, T.N. Goh, H. An, A. Maghbouli, Study on RCCI (reactivity controlled compression ignition) engine by means of statistical experimental design, Energy 78 (2014) 777–787.
[58] D.C. Montgomery, G.C. Runger, Applied Statistics and Probability for Engineers, John Wiley & Sons, 2010.
[59] R. Bahrampoury, A. Behbahaninia, Thermodynamic optimization and thermoeconomic analysis of four double pressure Kalina cycles driven from Kalina cycle system 11, Energy Convers. Manag. 152 (2017) 110–123.
[60] A. Arora, S. Kaushik, Theoretical analysis of LiBr/H2O absorption refrigeration systems, Int. J. Energy Res. 33 (2009) 1321–1340.
[61] A. Mohammadi, A. Kasaeian, F. Pourfayaz, M.H. Ahmadi, Thermodynamic analysis of a combined gas turbine, ORC cycle and absorption refrigeration for a CCHP system, Appl. Therm. Eng. 111 (2017) 397–406.
[62] A. Wang, S. Wang, A. Ebrahimi-Moghadam, M. Farzaneh-Gord, A.J. Moghadam, Techno-economic and techno-environmental assessment and multi-objective optimization of a new CCHP system based on waste heat recovery from regenerative Brayton cycle, Energy 241 (2022) 122521.
[63] A. Ebrahimi-Moghadam, A.J. Moghadam, M. Farzaneh-Gord, K. Aliakbari, Proposal and assessment of a novel combined heat and power system: energy, exergy, environmental and economic analysis, Energy Convers. Manag. 204 (2020) 112307.